CLINICAL RELEVANCE OF TERTIRARY LYMPHOID STRUCTURES ON TREATMENT RESPONSE IN MUSCLE INVASIVE BLADDER CANCER

NOUR HASSAN

Department of Experimental Surgery

McGill University

Montreal QC, Canada

June 2023

A thesis submitted to McGill University in partial fulfilment of the requirement of the degree of

Master of Science

I dedicate this work to tant May, Teta Magda, and Teta Tetto. You were never alone in this battle, and you never will be.

ACKNOWLEDGMENTS

I must start my acknowledgements by thanking the most important person in my life, even though nothing I say will ever do her justice. My mother raised me to believe that the only thing holding me back is how big I can dream. Someone from my background does not typically end up studying abroad, at McGill University of all places, but my mom never cared for typical. This thesis in its entirety is a thank you letter to you, Houba. Thank you for believing in me. Thank you for pushing me. Thank you for being there to cheer me on at every turn. Thank you for lifting me up after every fall. Thank you for never letting our circumstances dictate our ambition. Thank you for working day and night to make it possible. My heart is filled with pride today as I return to you with this work, and I know that yours is too.

I became interested in medical sciences after seeing my father operate on a patient for the first time. His skills, work ethic, and intelligence have always inspired me. This work would not have been possible without his endless sacrifice and support. I also want to thank my brother for showing interest and always asking questions about my research, even though he doesn't really care about science.

I joined this amazing lab by pure fate, and I couldn't have asked for a better team to be part of. I am eternally grateful to each and every member of the Kassouf team and will always consider myself part of this family. I would first like to thank Dr. Kassouf for giving me the opportunity to work on this project and present it in several conferences despite the short timeline. You challenged me in all the right ways and guided me with great vision and compassion throughout this project. I am very lucky to have had a chance to be trusted and mentored by you.

I worked on the bench next to Dr. Jose João Mansure almost every day for the past year, and I loved every minute of it. JJ, you brought so much joy to my heart and continued to lift me up at my worst moments. I am endlessly grateful for your invaluable mentorship, kindness, and patience with me. You encouraged me to stay curious and critical about science, so I thank you for making me the scientist and thinker that I am today. And I thank you for not giving up on me or this project during the difficult times.

Dr. Éva Michaud was a true role model to me. She led by example through her kindness and intelligence, going out of her way to make the lab a safe and fun learning space. Thank you Éva for making me feel heard, valued, and supported at the lab. You are a true gem of a scientist and a human being, and I learned so much just by watching you stand up for your ideas and advocate for what you believe in. Thank you for being there for me through the ups and downs.

I am the luckiest girl in the world for having the support system that I have. Thank you, John, for loving me through the good, the bad, and the ugly. Thank you, Alex, for listening to me rant about my data over Banh Mis. Thank you, Dylan, for helping me stay grounded and giving me a space to process my frustrations. Thank you, Momo, for making me laugh through the difficult times since 7th grade. In fact, my best friend Momo and his mom tant May have been calling me doctor since we were kids. This is not that degree, but I promise you it will happen someday.

Finally, I would like to thank the chair and the members of my research advisory committee, Dr. Elie Girsowicz, Dr. Peter Metrakos, and Dr. Luis Souhami for their time and valuable advice.

To begin, Bismillah.

STATEMENT OF INTEGRITY

I, Nour Hassan, attest that the work submitted represents solely my own efforts. I am aware of the University rules and regulations on plagiarism and subsequent penalties.

Table of Contents

ABSTRACT

Radical cystectomy (RC) is the standard of care for muscle invasive bladder cancer (MIBC). Radiotherapy (RT) is a bladder preserving option that offers patients comparable survival rates. However, up to 30% of patients require salvage RC. Furthermore, neoadjuvant chemotherapy (NAC) is given to some patients prior to underdoing RC, but most patients end up enduring treatment toxicities without benefit. Emerging evidence points to an important yet poorly understood link between response to therapy and the tumor microenvironment (TME). Notably, tertiary lymphoid structures (TLS) are being investigated as a potential local hub for mounting an immune response. These lymph-node-like structures are highly organized with a B cell zone surrounded by T cells. Mature TLS also have an active germinal center (GC) with follicular dendritic cells. A number of studies correlated TLS with improved outcomes in several types of solid cancers. Here, we explore the use of TLS and its associated immune TME as a predictive biomarker for response to RT and NAC in MIBC.

Hematoxylin and Eosin (H&E) stained formalin-fixed-paraffin-embedded sections of pre-RT and pre-NAC biopsy from 147 and 103 MIBC patients, respectively, were examined to identify TLS presence with confirmation from a pathologist. Subsequent multiplex immunohistochemistry (mIHC) staining with CD20 and CD3 to confirmed TLS presence, and CD21 and CD23 characterized TLS maturity. To investigate the interaction between TLS and TME, tissue microarrays were constructed, and gene expression profiles were obtained for 106 patients from the RT cohort using NanoString's Digital Spatial technology. Moreover, the TMA were stained by mIHC with CD20, Neutrophil Elastase, CD68, CD8, CD4, and FoxP3. Image analysis was performed on the Halo platform. The previously described TLS 12-chemokine signature was correlated to the immune infiltration and the patient outcomes.

H&E and subsequent mIHC revealed that 83% (n=118) and 85% (n= 88) of cases had TLS in the RT and NAC cohort, respectively. TLS presence alone had no association with response to RT or NAC, as well as no correlation with survival. However, we found that responders to RT had higher density and more mature TLS (Mann-Whitney test p=0.01 and p=0.026, respectively). However, CD21 expression was higher in germinal centers of non-responders (Mann-Whitney test p=0.04). Furthermore, high TLS density was associated with increased overall and cancer-specific survival (Log-rank test p=0.044 and p=0.034, respectively). We found a positive correlation between TLS density and infiltration of regulatory T cells in responders (Pearson's correlation, r=0.630, p=0.043) and a negative correlation with CD8+ cytotoxic T cells in non-responders (Pearson's correlation, r=-0.173, p=0.029). Finally, patients were clustered based on their expression of the 12-CK signature, with complete responders being enriched in the cluster with the highest expression of chemokines in the stroma, and non-responders in the cluster with the lowest expression in the tumor.

Our results point to a complex role of TLS in the context of response to RT and in relation to the TME. Overall, our study identifies a TLS profile that could serve as a selection criterion for patients who would benefit the most from RT to preserve their bladder.

RÉSUMÉ

La cystectomie radicale (CR) est le traitement standard pour le cancer de la vessie envahissant le muscle (CVIM). La radiothérapie (RT) est une option de préservation de la vessie offrant aux patients des taux de survie comparables. Cependant, jusqu'à 30% des patients nécessitent une CR de sauvetage. De plus, une chimiothérapie néoadjuvante (CNA) est administrée à certains patients avant de subir une CR, mais la plupart des patients subissent des toxicités liées au traitement sans bénéfice. Des preuves émergentes soulignent un lien important mais mal compris entre la réponse au traitement et le microenvironnement tumoral (TME). Notamment, les structures lymphoïdes tertiaires (TLS) font l'objet d'études en tant que centre local potentiel pour monter une réponse immunitaire. Ces structures semblables aux ganglions lymphatiques sont bien organisées, avec une zone de lymphocytes B entourée de lymphocytes T. Les TLS matures possèdent également un centre germinatif actif avec des cellules dendritiques folliculaires. Plusieurs études ont corrélé les TLS à une amélioration des résultats dans plusieurs types de cancers solides. Ici, nous explorons l'utilisation des TLS et de leur TME immunitaire associé en tant que biomarqueur prédictif de la réponse à la RT et à la CNA dans le CVIM.

Des sections d'échantillons de biopsie pré-RT et pré-CNA de 147 et 103 patients atteints de CVIM, respectivement, ont été examinées à l'aide de la coloration à l'hématoxyline et à l'éosine (H&E) sur des coupes fixées au formol et incluses en paraffine pour identifier la présence de TLS, confirmée par un pathologiste. Une coloration immunohistochimique multiplexe (mIHC) avec CD20 et CD3 a confirmé la présence de TLS, et CD21 et CD23 ont caractérisé la maturité des TLS. Pour étudier l'interaction entre les TLS et le TME, des microarrays de tissus ont été construits, et les profils d'expression génique ont été obtenus pour 106 patients de la cohorte RT en utilisant la technologie spatiale numérique de NanoString. De plus, les microarrays de tissus ont été colorés

par mIHC avec CD20, élastase, CD68, CD8, CD4 et FoxP3. L'analyse d'image a été réalisée sur la plateforme Halo. La signature de 12 chimiokines TLS précédemment décrite a été corrélée à l'infiltration immunitaire et aux résultats des patients.

H&E et la mIHC ont révélé que 83% (n = 118) et 85% (n= 88) des cas présentaient des TLS dans les cohortes RT et CNA, respectivement. La présence de TLS n'avait aucune association avec la réponse à la RT ou à la CNA, ni aucune corrélation avec la survie. Cependant, nous avons constaté que les répondants à la RT avaient une densité plus élevée et des TLS plus matures (test de Mann-Whitney p = 0,01 et p = 0,026 respectivement). Cependant, l'expression de CD21 était plus élevée dans les centres germinatifs des non-répondants (test de Mann-Whitney p = 0,04). De plus, une densité élevée de TLS était associée à une survie globale et spécifique au cancer plus longue (test du log-rank p = 0,044 et p = 0,034, respectivement). Nous avons trouvé une corrélation positive entre la densité de TLS et l'infiltration des cellules T régulatrices chez les répondants (corrélation de Pearson, r = 0,630, p = 0,043) et une corrélation négative avec les lymphocytes T cytotoxiques CD8+ chez les non-répondants (corrélation de Pearson, r = -0,173, p = 0,029). Enfin, les patients ont été regroupés en fonction de leur expression de la signature de 12 chimiokines TLS, les répondants complets étant enrichis dans le cluster avec la plus forte expression de chimiokines dans le stroma, et les non-répondants dans le cluster avec la plus faible expression dans la tumeur.

Nos résultats mettent en évidence le rôle complexe des TLS dans le contexte de la réponse à la RT et en relation avec le TME. Dans l'ensemble, notre étude identifie un profil de TLS qui pourrait servir de critère de sélection pour les patients qui bénéficieraient le plus de la RT pour préserver leur vessie.

Contribution of authors

This project was given to me by Dr. Wassim Kassouf. The experiments were designed under the guidance of Dr. Wassim Kassouf, Dr. Jose João Mansure, and Dr. Éva Michaud. Clinicopathological information was gathered by Dr. Ronald Kool, Jaleh Ebnealian, and I. The tissue microarrays were designed by Dr. Jose João Mansure, Dr. Rodrigo Skowronski, Dr. Fadi Brimo and Dr. Wassim Kassouf. Digital spatial profiling was done at Nanostring Technologies under the guidance of Dr. Jose João Mansure. Hematoxylin and Eosin staining for patients lacking diagnostic slides was done by me. Multiplex immunohistochemistry staining was optimized and executed by Fazila Chouiali at the RI-MUHC Histopathology platform under the guidance of Dr. Surashri Shine-Jadhav, Dr. Jose João Mansure, and I. Image analysis on Halo was performed by me. Statistical analysis and figures generation was done by me with the guidance of Dr. Jose João Mansure and Dr. Éva Michaud.

CHAPTER 1: Introduction

1.1 Bladder cancer

The bladder is a hollow, muscular organ located in the lower abdomen. It is positioned in the pelvic cavity, behind the pubic bone, and sits in front of the rectum in males or in front of the uterus and vagina in females. Its shape can vary depending on its filling state. The bladder has a flexible and expandable structure that allows it to store urine produced by the kidneys. It is composed of several layers of tissue, including the inner mucosal layer, a submucosal layer, a muscular layer called the detrusor muscle, and an outer layer of connective tissue. The arterial blood supply to the bladder comes primarily from branches of the internal iliac arteries, including the superior and inferior vesical arteries. These arteries form a rich vascular plexus within the bladder wall, ensuring an adequate blood supply. Lymphatic vessels in the bladder wall drain into regional lymph nodes, including the external and internal iliac lymph nodes, as well as the common iliac lymph nodes [1].

The main function of the bladder is to store and release urine. When urine enters the bladder from the kidneys through the ureters, the bladder expands to accommodate the increasing volume. The detrusor muscle contracts to maintain urinary continence and prevent leakage. When the bladder reaches its capacity or when it is appropriate to urinate, the detrusor muscle contracts more forcefully, while the urethral sphincter relaxes, allowing urine to be expelled from the body. The bladder also plays a role in signaling the brain when it is time to urinate. In terms of innervation, it receives nerve fibers from both the sympathetic and parasympathetic divisions of the autonomic nervous system. Sympathetic fibers arise from the lower thoracic and upper lumbar spinal cord levels, while parasympathetic fibers originate from the sacral spinal cord segments (S2-S4). These

nerve fibers regulate bladder function by controlling the relaxation and contraction of the bladder wall muscles, as well as the opening and closing of the bladder neck and urethral sphincters [1].

1.1.1 Epidemiology

Bladder cancer, also known as urological cancer or urinary bladder cancer, is the 10th most common cancer in the world with an estimated diagnosis of 573,278 cases in 2020, accounting for 3% of global cancer diagnoses [2]. The incidence rates are overall increasing but vary widely among countries with higher rates observed in developed countries compared to developing regions. In Canada, it is the 4th most common cancer in men and the 10th most common in women, which makes it the 5th most common cancer overall [3]. In fact, over three-quarters of bladder cancer cases are observed in men compared to women, with a mean age of onset greater than 65 years [2]. While the disease is more common in men, women were reported to have worse survival and treatment outcomes comparatively[4]. Bladder cancer accounts for 213,000 deaths every year, with Egypt having the highest mortality rate, making it the 9th leading cause of cancer death in men worldwide [5].

Bladder cancer incidence rates show geographic variations, with the highest rates observed in Southern and Western Europe, as well as North America. On the other hand, Central and South America, Africa, and Southeast Asia have the lowest reported incidence rates. Racial and ethnic differences also exist, as non-Hispanic white men have double the incidence rates compared to Hispanic and African American males [5].

The vast majority (90%) of bladder cancer cases, particularly in developed countries, originate from the urothelial cells found predominantly in the bladder but occasionally in the urinary tract. Squamous cell bladder cancer, which represents the remaining 10% of cases, is more common in Northern and sub-Saharan Africa and is believed to be linked to the parasite schistosomiasis [2].

Since 75% of cases are diagnosed as non-muscle invasive, bladder cancer is commonly associated with a good prognosis and survival rate of 73%. The other 25% of patients are diagnosed with muscle invasive bladder cancer (MIBC) or metastatic bladder cancer, the latter of which has a 5-year survival rate of only 16% [6]. Generally, bladder cancer poses a significant financial burden due to its high recurrence rate of 80%, making it the most costly cancer to treat per patient from diagnosis to death [7].

1.1.2 Risk factors

Several well-established risk factors contribute to the development of bladder cancer. These include physiological, environmental, and genetic factors [6].

The most significant risk factor is advanced age, due to extended exposure to carcinogens such as tobacco smoke and benzene, combined with an age-related deterioration of DNA repair function. The increased incidence in men compared to women could be explained by differences in lifestyle and exposures. The risk of bladder cancer may also be elevated in men with prostate enlargement and urinary retention, as the stagnant urine can contain carcinogenic substances [6].

Tobacco smoking is another important risk factor with a population-attributable risk of approximately 50%. Exposure to certain chemicals and occupational hazards such as aromatic amines, polycyclic aromatic hydrocarbons, and industrial substances like dyes, rubber, and textiles also increase the risk of bladder cancer. Chronic inflammation of the bladder, either due to recurrent urinary tract infections or long-term use of catheters, can contribute to the development of the disease since they can be drivers of cellular proliferation. Pelvic radiation and certain chemotherapy agents also increase the risk of bladder cancer [6].

Among genetic factors, family history of bladder cancer and certain genetic mutations can predispose individuals to the disease. Additionally, people with a history of certain inherited conditions, such as Lynch syndrome, are at an increased risk [6].

1.1.3 Etiology

Genetic causes play a role in the development of bladder cancer, and several gene mutations and alterations have been identified as contributing factors. Common mutated genes in bladder cancer include *TERT, TP53, HER2, PIK3CA, FGFR3,* and *HRAS* [8].

Among the most common mutations, *TERT* and *TP53* were found to be abnormally expressed in 70% and 56%, respectively. *TP53* encodes the p53 protein, which acts as a tumor suppressor [8, 9]. Mutations in *TP53* allows abnormal cell growth and was highly correlated with aggressive disease, indicating that it plays an important role in pathogenesis [8]. *TERT*, telomerase reverse transcriptase gene, is involved in DNA protection and cellular ageing. *TERT* mutations were found at different stages of bladder tumor development, suggesting that they occur early on during carcinogenesis [9].

The PI3K pathway controls cell metabolism, growth, proliferation, and survival and is the most studied signaling pathway in bladder cancer. Mutations in the *PIK3CA* gene, which codes for the p110α catalytic subunit of phosphatidylinositol 3-kinase (PI3K), are found in approximately 25% of non-muscle invasive bladder cancers (NMIBC). Also known as *ERBB2*, *HER2* is a receptor tyrosine kinase that is abnormally expressed in 32% of cases. In this pathway, overexpression of *EGFR*, *FGFR3*, *ERBB2* or *ERBB3* is associated with tumor grade, stage, and prognosis, suggesting that this pathway could be a driver of bladder tumor development and progression [8].

The *HRAS* gene, classified as a proto-oncogene, has the potential to transform normal cells into cancerous cells in various organs, including the bladder. HRAS gets altered through a somatic

mutation in the bladder, specifically a substitution of a glycine with a valine. This mutation prompts uncontrolled cell division and tumor formation [9]. Furthermore, HRAS gene mutations have been associated with the progression of bladder cancer and an increased risk of tumor recurrence following treatment [9].

1.1.4 Symptoms

The primary manifestation of bladder cancer is visible, gross hematuria, although patients may also present with isolated microscopic hematuria, characterized by the presence of at least 3 red blood cells per high-power field in a urinalysis. The risk of bladder cancer is estimated to be around 4% in individuals with microscopic hematuria and approximately 16.5% in those with gross hematuria [6]. In cases of gross hematuria, the urine appears dark red or rusty, and the patient may present with other obstructive symptoms like vesical irritability, double voiding, overflow continence, and lower abdominal pain. Advanced stages of bladder cancer can give rise to symptoms such as urinary retention, loss of appetite, weight loss, and lower back pain. Unfortunately, these symptoms can be confused for urinary tract infections especially by women, leading to potential misdiagnosis and delays in identifying the underlying bladder cancer [10].

1.1.5 Diagnosis

The current American Urological Association guidelines recommend a personalized approach in hematuria evaluation based on the patient's risk of having bladder cancer. This approach is a response to the relatively infrequent discovery of malignancy during evaluation, as well as the invasive nature of cystoscopy, the radiation exposure from cross-sectional imaging, and the associated expenses involved in conducting these procedures [6].

High-risk individuals undergo cystoscopy to assess the lower urinary tract. Cystoscopy is a procedure performed using a thin, flexible camera that is inserted through the urethra. Enhanced cystoscopy techniques, such as narrow-band imaging or blue light cystoscopy, provide a better accuracy in detecting bladder tumors during both diagnostic cystoscopy and endoscopic resection, offering improved sensitivity and specificity [6].

Transurethral resection of bladder tumor (TURBT), also known as endoscopic resection, serves both diagnostic and potential therapeutic purposes for newly identified bladder tumors. Its two objectives are to remove all visible tumors and to pathologically stage the disease. In cases where the resection is incomplete, detrusor muscle is absent in the pathological sample, or the disease is classified as high-risk stage Ta or T1, it is recommended to undergo a repeat TURBT within 4 to 6 weeks. In such situations, the probability of having residual disease is as high as 51% in T1 disease, and the potential for the disease to be upstaged to muscle-invasive is 8% in subsequent TURBT [6].

Cross-sectional imaging techniques such as computed tomography (CT) or magnetic resonance imaging urogram (MRI) are employed to examine the upper urinary tract in patients exhibiting gross hematuria and high-risk microscopic hematuria. On the other hand, renal ultrasound is used for patients with low- and intermediate-risk microscopic hematuria. While routine imaging for initial staging is not typically conducted in patients suspected of having bladder cancer, the VI-RADS system (Vesical Imaging-Reporting and Data System) can be used to detect muscle invasive disease [6].

Gross hematuria and posttreatment surveillance are assessed by urine cytology. This test involves the examination of malignant urothelial cells, primarily of high grade, which tend to detach more easily than low-grade malignant cells. Although several urine biomarkers have

received approval from the US Food and Drug Administration (FDA) and are beneficial as additional tools, none of them possess the necessary diagnostic accuracy to replace cystoscopy [6].

1.1.6 Staging and grading

The objective of histological tumor classification is to categorize patients into distinct groups based on their prognosis and to implement appropriate management strategies for each group. Bladder cancer is initially classified based on the cell type that gave rise to the tumor. Approximately 90% of all bladder cancer cases are urothelial or transitional cell carcinoma, but squamous cell carcinoma and adenocarcinoma are also possible although less common diagnoses variants. The next step in diagnosis is an assessment of stage and grade [6].

The pathological staging of bladder cancer involves the assessment of the extent and spread of the tumor within the bladder and surrounding tissues (figure 1). The most commonly used staging system for bladder cancer is the TNM system, which stands for Tumor, Node, and Metastasis. The T stage refers to the extent of the primary tumor penetration into the bladder wall. It ranges from T0 indicating no evidence of disease, to non-muscle invasive bladder cancer (NMIBC) including carcinoma in situ (Tis), non-invasive papillary carcinoma (Ta), and tumor invading the lamina propria (T1). MIBC is classified as T2. T3 bladder cancer involves invasion of the of fat surrounding the muscle layer, and T4 bladder cancer involves nearby organs and structures (figure 1). The N stage indicates the involvement of regional lymph nodes. It is categorized as N0, which indicates regional lymph node involvement or N1-N3 with increasing degree of lymph node involvement. The M stage represents the presence or absence of distant metastasis, where M0 is negative while M1 is positive for distant metastases [11].

The categorization of urothelial tumors into low grade and high grade was initially included in the World Health Organization (WHO) 2004 classification and continues to be a component of the

2016 classification system. Grading describes the degree of resemblance to the cell of origin, where a high-grade tumor is less reminiscent of the parent cell and is associated with more aggressive disease [12]. Low grade tumors are characterized by *HRAS* and *FGFR3* mutations, whereas high grade tumors are associated with *TP53* abnormalities [11]. pTa and pT1 tumors could be either classified as low grade or high grade, while MIBC is considered high grade. Since lymphovascular invasion and metastasis may occur with pT1 tumors as they grow into the subepithelial layer, pathologists often classify them as high grade regardless of how atypical they are [12].

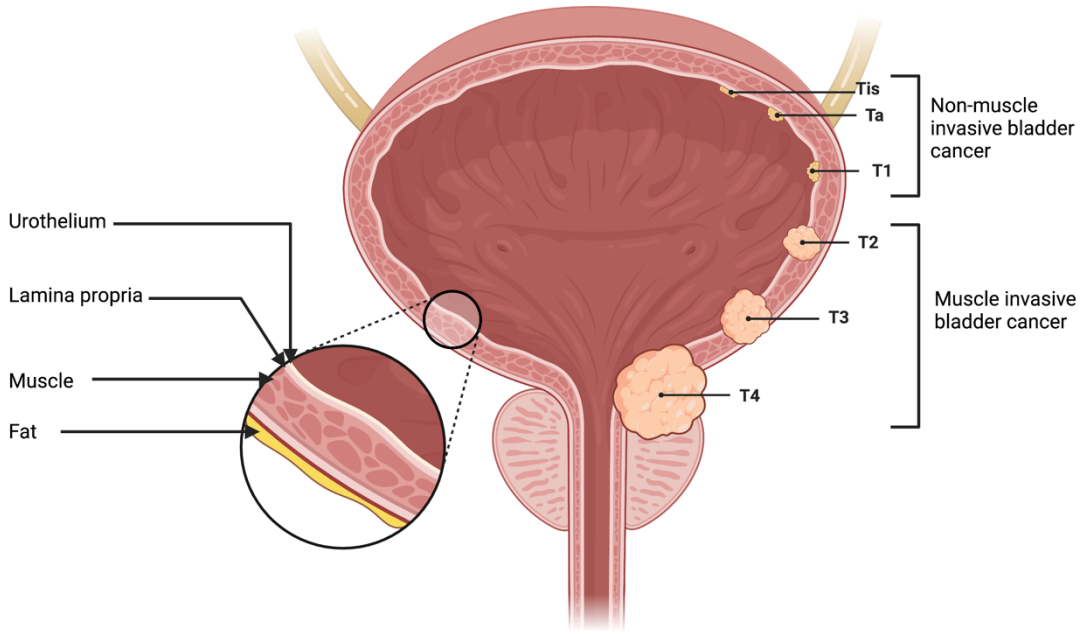

Figure 1: Staging of bladder cancer (figure created with Biorender.com)

1.2 Management of MIBC

MIBC accounts for up to 30% of bladder cancer cases. The standard treatment for patients with MIBC includes neoadjuvant therapy followed by radical cystectomy, pelvic lymph node dissection, and urinary diversion. In selected cases, bladder-sparing approaches such as chemoradiation or partial cystectomy may be considered.

1.2.1 Neoadjuvant chemotherapy

Neoadjuvant chemotherapy (NAC) refers to any systemic chemotherapeutic treatment delivered to the patient prior to surgery and/or radiation. This approach allows for both the control of the primary tumor and the early treatment of any micrometastases, therefore decreasing the risk of relapse. Breast, pancreatic, and gastric cancers are among many malignancies where NAC is the standard of care [13-15]. In the 1980s, cisplatin-based NAC was initially examined as a treatment option for MIBC [16]. Since then, several clinical trials demonstrated the survival benefits of adding NAC compared to radical cystectomy alone. Cisplatin-based NAC became the standard of treatment following a 2005 meta-analysis showing a 5-year survival benefit of 5% [17]. In the context of MIBC, the two most common NAC regimens are a combination of methotrexate, vinblastine, doxorubicin, and cisplatin; (MVAC) and gemcitabine plus cisplatin (GemC).

The SWOG-8710 trial was the first randomized clinical trial that demonstrated the benefit of adding neoadjuvant MVAC in MIBC. 307 patients with MIBC were randomly assigned to receive either MVAC followed by RC or RC alone. The trial's results, published in 2003, showed a significant improvement in overall survival (OS) for patients who received MVAC, with a 33% reduction in the hazard ratio for death [18]. Shortly thereafter, MVAC became incorporated in the standard of care for MIBC. The treatment is typically administered in 3-6 cycles, lasting 3 weeks

each. The drugs are given sequentially in the following manner: Methotrexate is administered on day 1, followed by Vinblastine, Doxorubicin and Cisplatin on day 2, then Methotrexate and Vinblastine again on days 15 and 22 [19]. Treatment with MVAC, however, is associated with a high risk of adverse events and toxicities, including but not limited to neutropenia and its subsequent susceptibility to infectious complications. Additionally, considerable mucositis resulting in difficulties with eating and drinking may lead to weight loss and overall weakness. Other observed toxicities include nausea, vomiting, renal impairments, cardiac complications, and neurological manifestations. These side effects pose particular challenges for elderly patients, who frequently present with comorbidities and constitute a substantial proportion of the MIBC patient population. Moreover, MVAC is linked to a toxic mortality rate ranging from 3% to 4% [20]. One strategy to overcome those issues is the dose dense administration of MVAC (ddMVAC), which is given in 2-week cycles with granulocyte colony stimulating factor (G-CSG) to protect from neutropenia [21]. Two small phase II studies proved the efficacy and tolerability of ddMVAC in MIBC patients, which quickly became the preferred dosing strategy [22, 23].

The other common NAC regimen is GemC. Initially, GemC was given to metastatic BC patients during a trial by von der Maase *et al*. The study included 405 patients and found that GemC was non-inferior to MVAC in terms of OS and response rates. Additionally, GemC was associated with a significantly lower incidence severe toxicities, making it a more tolerable treatment option [20]. Subsequently, a multi-center retrospective study confirmed that there was no difference in outcomes between the two regimens [24]. Seeing its higher tolerability, GemC was adopted in the neoadjuvant setting for MIBC management without prospective trials. GemC is typically given in 4-6 cycles, lasting three weeks each.

Recently, studies comparing ddMVAC with GemC have been conducted in patients with localized MIBC. The SWOG-1314 trial included 167 patients and found comparable rate of progression free survival (PFS), OS, and pathological complete response (pCR) between the groups. However, the French Association of Urology V05 VESPER trial of 437 randomized patients found a better 3-year PFS rate as well as a higher rate of organ confined response in patients receiving ddMVAC compared to GemC [25]. More recently, a nationwide cohort study from Korea showed no difference in OS between patients treated with MVAC and GemC [26].

It is important to note that approximately 50% of MIBC patients are ineligible to receive cisplatin-based therapy due to age and/or disease-related comorbidities. Cisplatin-ineligibility criteria include impaired renal function, class III heart failure, grade ≥2 hearing loss, and grade ≥2 neuropathy. As an alternative to GemC, combination of carboplatin and gemcitabine has been studied in retrospective analyses, showing pCR rates of 20% to 30% in MIBC patients. Other alternatives, such as paclitaxel, carboplatin, and gemcitabine, consistently demonstrated lower pCR rates compared to cisplatin-based regimens. Therefore, the National Comprehensive Cancer Network guidelines do not recommend non-cisplatin-based NAC. In some patients who meet specific renal function criteria, split-dose GemC may be a tolerable alternative [27].

1.2.2 Radiation therapy

Radiotherapy (RT) involves the delivery of high-energy beams to specifically cause DNA damage and kill cancer cells. The dose of radiation to a biological material is defined at the amount of energy per unit mass (1 Joule/kg= 1 Gray or Gy) and includes both x-rays and gamma-rays. RT utilizes ionizing radiation that can break molecular bonds in tissues by ionizing atoms through the removal of electrons. This process primarily affects rapidly proliferating cells, which makes cancer cells more susceptible to its damaging effects [28]. RT has demonstrated effectiveness in achieving

local tumor control for several cancers, such as lung, head and neck, and breast cancer; either as a monotherapy or in combination with other treatments [29].

From 1975 to 2002, various studies explored the use of radical external beam RT in the treatment of muscle MIBC. RT achieved a complete response in over 50% of patients, but only 30-50% of them maintained this response without recurrence, and about 50% of those who initially responded experienced distant metastases. Besides, preoperative RT did not demonstrate significant oncological benefits in terms of disease dissemination during surgery, according to a meta-analysis [30].

Currently, RT is given as a component of bladder-preserving trimodal therapy (TMT). In 1993, a prospective study where patients were treated with TURBT followed by chemotherapy combination of 5-fluorouracil and cisplatin with split-course RT reported a 3-year disease-free survival rate of 62%. The largest study of bladder preservation therapy was published in 2002 by Rödel and colleagues where they treated and followed 415 patients over 18 years. Over 80% of patients preserved their bladder and the 10-year disease-specific survival was 42%. Several additional studies have shown favorable 5-year survival rates ranging between 48% and 65%, with a notable percentage of patients retaining their original bladders.

In the context of TMT, the standard RT regimen consists in delivering external beam radiation therapy to the bladder and pelvic lymph nodes, starting with a dose of 40 Gy, followed by boosts to the bladder up to 54 Gy and the tumor up to 64-65 Gy. There have been recent advancements in hypofractionated treatment regimens, which aim to reduce the overall duration of therapy while achieving comparable results in terms of side effects and disease management. These modified regimens typically involve delivering a total radiation dose of 50 to 52.5 Gy,

divided into 20 fractions, over a period of 4 weeks. In many cases, it is combined with weekly gemcitabine administration [31].

The only prospective randomized trial comparing RC with TMT, the SPARE trial, was terminated early due to the lack of accrual [32]. The present guidelines endorse the use of TMT as a substitute for radical cystectomy but highlight the importance of selecting suitable patients. Optimal candidates should be capable of undergoing a complete TURBT and have small, isolated tumors with minimal carcinoma in situ and absence of hydronephrosis. These requirements limit the number of suitable patients for bladder preservation to about 6-30% of individuals with MIBC [33, 34]. In any case, TMT has been underutilized due to concerns about recurrence, inadequate treatment of regional lymph nodes, and the potential complications associated with salvage cystectomy following high-dose pelvic irradiation [33].

1.3 Effects of chemotherapy and radiation therapy on cancer

Chemotherapy and radiation therapy can induce tumor cell death in several ways, both directly and indirectly. Intrinsic and extrinsic pathways contribute to the sensitivity or resistance of the tumor cells to treatment. In particular, the tumor microenvironment plays a critical role by providing a supportive or inhibitory niche for tumor progression.

1.3.1 Mechanisms of treatment-induced cytotoxicity

By preferentially targeting rapidly dividing cells, radiotherapy and chemotherapy have direct cytotoxic effects on tumor cells. Tumor cell death can take place in several ways: apoptosis, autophagy, mitotic catastrophe, and necrosis.

Description of cytotoxic mechanisms:

Apoptosis, also called programmed cell death, can be caused by two signaling pathways. These consist of the intrinsic pathway, also called mitochondria-mediated pathway, which responds to intracellular stress signals like DNA damage, high levels of reactive oxygen species (ROS), viral infection, or activation of oncogenes; and the extrinsic pathway that is triggered by an external ligand-receptor binding on plasma membrane. Both pathways activate caspases - proteolytic enzymes responsible for swift degradation of cellular organelles and architecture, leading to apoptotic cell death [35].

Activation of autophagy depends on various stimuli such as nutrient deprivation, differentiation, and developmental triggers. In reaction to metabolic stress, cellular proteins and organelles are enclosed in double-membrane structures termed autophagosomes, which fuse with lysosomes for degradation. While autophagy can ensure cell survival during starvation situations, extreme autophagic activities can trigger cell death [35].

Mitotic catastrophe refers to cell death that occurs during mitosis because of deficient cell-cycle checkpoints, particularly DNA structure and spindle assembly checkpoint. This results from inadequate chromosomal segregation during sister chromatid separation, leading to an irreversible trigger for cell death [35].

Necrotic cell death is characterized by cellular swelling, organelle damage, and rupture of the plasma membrane, leading to the release of cellular contents into the extracellular space. Unlike apoptosis, necrosis is typically considered an uncontrolled and accidental process. It can be triggered by various factors, such as physical trauma, severe oxidative stress, toxins, or ischemia [35]. Recently, an alternative form of programmed necrosis called necroptosis has been shown to take place when the caspase-8-dependent apoptotic pathway is blocked. Activation of necroptosis

is initiated by immune ligands and is confined to certain types of tissues expressing RIPK3/MLKL [36].

Cytotoxic mechanisms of chemotherapy:

Each of the chemotherapeutic agents used in MVAC and GemC can employ one or more of those mechanisms to induce tumor cell death. Cisplatin is a platinum-based agent that can cross link purine bases of DNA, causing cell cycle arrest. Failure of DNA damage repair results in the accumulation of the DNA adducts, leading to the induction of apoptosis in the cell [37]. Some studies reported that higher doses of cisplatin can also cause necrotic cell death [38].

As previously discussed, gemcitabine is used along with cisplatin in the GemC regimen. Gemcitabine is a nucleoside analog that causes tumor cell death through apoptosis and autophagy. Firstly, the incorporation of gemcitabine into DNA inhibits synthesis by blocking DNA polymerase. The drug can also self-potentiate by reducing the intracellular pool of nucleotides, hence increasing its chance of integrating in the DNA. Those events result in the activation of caspase signaling, leading to apoptosis [39]. Secondly, gemcitabine can induce the expression of vacuole membrane protein-1 (VMP1), which activates autophagosome formation and leads to autophagy [40].

The drugs in the MVAC regimen induce cell death in a variety of ways. Methotrexate is an anti-folate synthetic compound that is used to treat multiple autoimmune conditions and cancers. The molecule acts by blocking the folate cycle, leading to a disruption in cellular metabolism and proliferation. Ultimately, DNA synthesis becomes inhibited due to insufficient nucleotides, and apoptosis is triggered [41].

Doxorubicin is an antibiotic agent that can cause apoptosis, autophagy, and necrosis [42]. The molecule is an inhibitor topoisomerase II, thereby blocking DNA repair. It can also cause the release of ROS, which leads to membrane damage, DNA damage, and triggers cell death [43].

Vinblastine is an alkaloid that binds tubulin, hence preventing microtubule formation. This results in cell cycle checkpoint inhibition, leading to mitotic catastrophe [35, 44].

Cytotoxic mechanisms of radiation therapy:

Ionizing radiation used in RT can either directly cause DNA damage or produce free radicals that cause DNA damage. This damage can take the form of single strand breaks or double strand breaks by disrupting the sugar-phosphate backbone of DNA. Additionally, radiation can impair nucleotide bases leading to the distortion of the DNA double-helix configuration, as well as induce DNA-protein cross linkage [45]. Following DNA damage, tumor cells can undergo cell death by apoptosis, mitotic catastrophe, or necrosis.

Several pathways are involved in radiation-induced apoptosis. Strand breaks will trigger the DNA repair machinery, which will inevitably fail to control the excessive damage and trigger apoptosis instead. Both the intrinsic and extrinsic pathways could be engaged, leading to caspase dependent degradation of cellular content. The intrinsic pathway is heavily mediated by p53, a transcription factor that upregulates downstream pro-apoptotic target genes such as Bax. The extrinsic pathway involves the activation of death receptors such as FasR and TNFR1[45].

Mitotic catastrophe is another main cause of radiation-induced cancer cell. RT can cause tumor cells to prematurely enter mitosis, an event that would be more likely to happen with a p53 mutation due to a dysfunctional G2/M checkpoint [45].

Although less common, cancer cells can also die by necrosis at higher doses of RT [45]. Radiation-induced necroptosis has also been described in certain settings [46].

1.3.2 Immune response to treatments

The tumor microenvironment (TME) is composed of the vasculature, extracellular matrix, secreted factors, and various non-cancerous cells surrounding the tumor. Immune cells make up a principal and active compartment of the TME that could be both tumor promoting and suppressive. The recognition of this dual facet was reflected by adding "evading immune destruction" and "tumor-promoting inflammation" as two immune hallmarks of cancer in 2011 [47]. Additionally, the tumor immune microenvironment (TIME) could directly influence treatment response. NAC and RT cause cell stress, which could induce immunogenic cell death and several immune modulation mechanisms. RT could also trigger a systemic anti-tumoral immune response, a phenomenon known as the abscopal effect.

Immunogenic cell death (ICD) is a regulated form of cell death that stimulates an immune response against dying cells. During ICD, cancer cells undergo specific molecular changes that make them recognizable to the nearby immune cells, including the release of damage-associated molecular patterns (DAMPs) and cytokines. Those include molecules like adenosine triphosphate (ATP), the pro-inflammatory protein high mobility group box 1 (HMGB1), the heat shock protein (HSP), and calreticulin (CRT). Additionally, ICD leads to the exposure of tumor-associated antigens that can be recognized by dendritic cells (DC), inducing their activation and maturation. What follows is a cascade of events involving antigen presentation and resulting in the mounting of an adaptive immune response against tumor cells [48].

Certain MIBC NAC agents have been shown to trigger ICD. Evidence from *in vivo* studies shows that gemcitabine can activate natural killer (NK) cells through ICD [49]. Similarly, doxorubicin-induced ICD elicits the infiltration of CD4+ helper T cells and CD8+ cytotoxic T cells, which limits tumor growth [49]. RT can result in ICD in two ways. Firstly, ROS production

and endoplasmic reticulum damage cause the release of DAMPs that triggers the ICD cascade. RT also induces ICD via the interferon type I (IFN-I) response. Double stranded DNA breaks induce cGMP generation that activates the STING–TBK1–IRF3 pathway (STING: stimulator of interferon genes; TBK1: TANK-binding kinase 1; IRF3: interferon regulatory factor 3). This leads to INF-I secretion that promotes DC maturation, hence resulting in an anti-tumoral CD8+ mediated response [50].

Treatment-induced cell stress could also lead to immune modulations that stimulate the TIME to act against cancer cells. Chemotherapy drugs can enhance the production of molecules that facilitate the interaction between immune cells. This includes the pro-apoptotic molecule Fas and tumor necrosis factor (TNF)-related apoptosis-inducing ligand (TRAIL) receptors. They could also enhance antigen presentation, making the remaining tumor cells more susceptible to elimination by immune cells. Additionally, certain chemotherapeutic agents directly stimulate the immune system, leading to the maturation and increased cytotoxic abilities of specific immune cell populations [51].

Cisplatin, gemcitabine, and doxorubicin have been shown to increase tumor cell expression of the Major Histocompatibility Complex class-I (MHC-I), which is necessary for the recognition and subsequent elimination of tumor cells by CD8+ cytotoxic T cells [51]. Furthermore, those drugs can increase the cytotoxic abilities of said cells through increased Granzyme-B secretion/production/release. Cisplatin has also been shown to inhibit immunosuppressive populations, such as regulatory T cells (Treg) and myeloid-derived suppressor cells (MDSC). Additionally, doxorubicin increases the expression of CD86 on B cells, which provides a costimulatory signal for T cell activation [52].

Similarly, RT can oppose immune evasion and enhance recognition of tumor cells by cytotoxic immune cells. This is done by increasing the levels of MHC-I and upregulating the expression of co-stimulatory molecules CD80/CD86 to activate CD8+ T cells; and increasing the expression of Natural Killer Group 2D (NKG2D) receptor stress ligands to activate NK cells. RT also promotes the release of Intracellular Adhesion Molecule 1 (ICAM-1) and Vascular Adhesion Molecule 1 (VCAM-1), facilitating lymphocyte attachment to blood vessel walls. In addition, it stimulates the production of pro-inflammatory cytokines and chemokines that recruit CD8+ cytotoxic T cells and Type 1 Helper (Th1) cells [53]. Finally, the INF-I released as a result of STING activation limits the immunosuppressive functions of Treg [50].

The abscopal effect refers to the occurrence where RT administered at a specific location prompts a systemic immune response against tumors throughout the body. Initially referred to as the "bystander effect," this phenomenon was initially observed *in vitro* when researchers discovered that reactive oxygen and nitrogen species produced during RT could cause DNA damage in distant non-irradiated cells. Evidence supports a T-cell mediated mechanism of the abscopal effect [54]. After irradiation, dying tumor cells release neoantigens, which can be taken up by antigen-presenting cells (APC) and presented to CD8+ T cells in the lymph nodes. Activated T cells can then recognize, infiltrate and attack both the primary tumour and non-irradiated tumour metastases [54]. The abscopal effect has been described in both preclinical and clinical settings. Several case reports demonstrate a systemic clinical response following local delivery of RT [55, 56]. Of note, our group has shown that treating bladder tumor-bearing mice with a combination of immune checkpoint inhibitors and RT lead to a size reduction of radiated and distant tumors [57].

1.3.3 Mechanisms of resistance:

Nonresponse to NAC is driven by chemoresistance. Mechanisms that determine chemoresistance fall into three categories: reducing DNA damage by chemotherapy, increasing cell survival by inhibiting apoptosis, and modulating the TME [58]. Cancer cells can employ a variety of mechanisms to ensure that chemotherapy-induced DNA damage is kept to a minimum. Not only can cellular uptake of the drug be reduced, but cancer cells can also activate a detoxification machinery by expressing transporters on their membrane to pump out toxic molecules. This is particularly relevant in the case of cisplatin, where cells expressing copper-transporting P-type adenosine triphosphatase ATP7B are highly resistant [59]. Increasing DNA repair capacity is also important in resistance. For instance, the ERCC1 enzyme, which is involved in nucleotide excision repair, is overexpressed in cisplatin resistant cancers [59]. Chemoresistance is also driven by the inhibition of apoptosis, which can be achieved by disrupting p53, hence preventing cell cycle arrest and death. Moreover, apoptotic genes such as Bcl-2 and FASL can be downregulated. Finally, chemoresistance can be affected by several elements of the TME, including the extracellular matrix [59].

Approximately 25% of patients receiving TMT will not respond to radiation therapy and have disease persistence or local recurrence [60]. This is driven by radioresistance mechanisms that allow tumor cells to survive and cause recurrence. One of the primary mechanisms of resistance involves DNA damage repair pathways. Tumor cells can upregulate DNA repair enzymes to fix the damage induced by radiation. Additionally, alterations in cell cycle checkpoints, particularly the G1/S and G2/M checkpoints, can contribute to resistance by allowing cells with damaged DNA to continue dividing. Activation of pro-survival signaling pathways, including PI3K/AKT and MAPK/ERK, promotes cell survival and reduces the susceptibility of cancer cells

to radiation-induced cell death [58]. Furthermore, the inflammation resulting from RT induces cancer-associated fibroblasts (CAF) activation in the TME, which drive tissue remodelling and repair processes. Finally, hypoxic tumor microenvironments and inadequate oxygen supply limit the effectiveness of RT, as oxygen is crucial for the generation of ROS that mediate radiation-induced cell death. Hypoxia also increase Hypoxia-inducible factor 1α (HIF1α) expression, which independently causes radioresistance by promoting cell survival[61].

1.4 Tertiary lymphoid structures:

Tertiary lymphoid structures (TLS) are *de novo* assemblages of lymphocytes, DC, and stromal cells that resemble secondary lymphoid organs (SLO). They have been documented under pathological conditions of chronic inflammation, such as autoimmune disorders, infectious diseases, transplanted organ rejections, and malignancies. TLS have been of particular interest in cancer research since being first identified in non-small cell lung carcinoma (NSCLC), where their presence was associated with favorable outcomes[62]. They have been investigated as predictive and prognostic biomarkers, as well as potential hubs for mounting an effective anti-tumoral immune response. In MIBC, TLS have been identified and studied mainly in the context of immunotherapy; however, their specific functions remain elusive for the most part.

1.4.1 Lymphoid neogenesis

Most of our current knowledge of TLS formation, or lymphoid neogenesis, was inspired by known mechanisms of lymph node (LN) formation during embryogenesis, a process termed lymphoid organogenesis. Lymphoid organogenesis is contingent upon collaborative interactions between two types of cells: stromal lymphoid tissue organizer (LTo) cells, gp38+ fibroblasts precursors of fibroblast reticular cells (FRCs) and follicular dendritic cells (FDCs), and lymphoid

tissue inducer (LTi) cells of hematopoietic origin [63]. Communication between those cells occurs primarily through the lymphotoxin (LT) α1β2 ligand, expressed on the surface of LTi cells, and the LTβ receptor (LTβR), expressed on LTo cells[64]. This interaction results in the expression of adhesion molecules and chemokines, such as CC-chemokine ligand 19 (CCL19), CCL21 and CXC-chemokine ligand 13 (CXCL13), which are critical for attracting and retaining more LTi and immune cells at the location where LN are forming [64]. LTβR signaling also leads to the expression of peripheral node addressin (PNAd) on endothelial cells that form high endothelial venules (HEVs), specialized vessels that permit the entry of lymphocytes and dendritic cells into LN [63].

The cellular actors in LN development have been targeted to better understand their relevance in TLS development. Several immune cells expressing RORγt, a transcription factor commonly expressed on LTis, have been suggested as equivalent in lymphoid neogenesis [65-67]. Among them, a subset of innate lymphoid cells (ILC)-3 have been shown to trigger LTαβ and adhesion molecule expression and were associated with TLS formation in NSCLC [65]. However, evidence from other disease models suggests that RORγt expressing cells are not necessary for TLS formation [68-70]. For example, mice that lack the RORγt murine equivalent can form TLS in the colon and the lung under inflammatory conditions [68, 70]. Moreover, several RORγt$^-$ immune populations have been identified as possible LTi surrogates [68, 71-74]. In a melanoma mouse model, CD8+ T cells and NK cells were shown to secrete the cytokines responsible for lymphoid neogenesis [73]. The role of CD8+ T cells was further confirmed as the mediators of CAF network formation that mechanically supports TLS [74]. Finally, TLS forming in aging mouse bladder have been linked to CXCL-13 secretion by macrophages [72].

As for LTos, fibroblast populations have been identified as likely candidates for this role. Isolated VCAM-1+ CAF assemble into a reticular network and are sufficient to induce the formation of TLS in subcutaneous tumors that would otherwise not develop them [74]. Other cell populations that express SLO-associated chemokines could also assist in tissue organization [75-77]. For instance, follicular helper T cells (Tfh) were shown to produce CXCL13 in breast cancer patient tissues [76]. Similarly, in ovarian cancer, B cells and macrophages were the principal sources of CXCL13 [75].

Despite being necessary for LN organogenesis, evidence of the role of lymphotoxin signaling in lymphoid neogenesis remains inconclusive. On one hand, several studies support its implication in TLS formation. Targeting an antibody-LTα fusion protein directly to LTα-deficient mice bearing melanomas induced the formation TLS and PNAd+ HEV in the vicinity of the tumor and lead to a strong adaptive anti-tumoral immune response, despite the animals lacking SLO [78, 79]. Moreover, LTβ produced by DC has been found abundant in human breast tumors with a high density of HEV [80]. LIGHT, a pro-inflammatory cytokine and an alternative LTβR ligand, has also been associated with the neogenesis of cancer-associated TLS [81-85]. Notably, by targeting LIGHT to tumor vessels via a vascular targeting peptide (VTP), Johansson *et al*. were able to demonstrate a remodeling of the tumor vasculature and induction of TLS in a pancreatic cancer mouse model [84]. Nevertheless, other studies show that lymphoid neogenesis may not always depend on lymphotoxin signaling. Early studies in Ltα-deficient mice lacking SLO demonstrated the formation of inducible bronchus-associated lymphoid tissue (iBALT), a form of TLS that results from lung inflammation [86, 87]. Those iBALT were similar in size to the ones observed in wild-type mice, despite having a primitive organization with intermixed B and T cells [86]. More interestingly, they were able to mount an antigen-specific immune response when the mice

were challenged with influenza virus [87]. Further investigations showed that iBALT formation is independent of lymphotoxin signaling. Instead, interleukin-17 (IL-17) is responsible for triggering the expression of chemokines that lead to the assembly of immune cells [70].

Chemokines are key players in the induction and maintenance of both SLO and TLS. Studies of transgenic mice where ectopic expression of different chemokines was induced are particularly valuable to understand their roles. Each of CXCL13, CCL19, and CCL21 was independently and sufficiently capable of triggering lymphoid neogenesis but resulted in morphologically different structures. CXCL13 expression led to a high frequency of B cell infiltrates of all sizes that lack FDC networks. CCL19 recruited small aggregates composed of lymphocytes and DC and containing HEV and stromal cells. CCL21 induced larger and more organized TLS in the pancreas compared to CCL19 but was unable to induce them in the skin [88, 89]. Those findings suggest that CCL21 plays an important role in the structural organization of TLS, whereas CCL19 is more involved in lymphocyte recruitment. Those chemokines have also been described during lymphoid neogenesis in human cancer [90, 91]. In fact, in human lung cancer tissue, CCL19, CCL21, and CXCL13 were highly expressed inside tumor-associated TLS [90].

1.4.2 Organization and composition

TLS are heterogenous structures in terms of cellular composition and organization. In their most primitive form, TLS may consist of loosely aggregated B and T cells without well-defined compartments. Mature TLS, on the other hand, are architecturally similar to follicles in SLO, containing a delineated outer T cell zone and an inner B cell zone with a germinal center (GC) marked by the presence of FDC [92]. TLS can also contain FRC networks, DC, macrophages and HEV.

B cells make up the largest compartment of TLS and can be found by staining with the pan markers CD19 or CD20 (figure 2) [93]. In immature structures, called early TLS, naïve B cells are the predominant population. As they have not yet encountered their cognate antigen, they can be identified by the high expression of IgD [93, 94]. In fully mature structures, B cell follicles are marked by the presence of a GC where B cells undergo class switching and maturity affination. Those GC B cells are characterized by the high expression of activation-induced cytidine deaminase (AID), the key enzyme in somatic hypermutation and conversion of immunoglobulin genes [94]. Since they are highly proliferative, they also express Ki67 [94]. A study has also noted the presence of an antigen-presenting B cell subtype in the germinal center of cancer-associated TLS that was marked by the expression of CD86 [95]. Derived from mesenchymal cells, FDC form networks in the B cell zone that support the GC reaction. In primary follicle-like TLS, an intermediate stage of maturation, FDC express CD21, the complement receptor 2 that can trap immune complexes for antigen presentation. In addition to CD21, FDC in secondary follicle-like TLS upregulate CD23, the low-affinity Fc receptors for IgE involved in antibody feedback regulation in B cells [96, 97].

CD3+ T cells surround the B cell compartment of TLS (figure 2) [92]. Within the T cell zone, CD4+ C-X-C motif chemokine Receptor 5 (CXCR5) + Tfh are the dominant subset [76, 92]. Tfh interact with B cells during GC reaction, promoting somatic hypermutation and maturation of B cells into high-affinity antibody-producing plasma cells [98]. Moreover, Tfh promote the anti-tumoral functions of CD8+ cytotoxic T cells, which are found in the T cell zone of TLS [99, 100]. FoxP3+CD4+ regulatory T cells and CD4+ Th1 cells could also be present [92, 101]. Mature DC, marked by CD83 or DC-LAMP, carry out antigen presentation in the T cell zone [101]. Finally, CD68+ macrophages are distributed throughout to remove apoptotic cells [102].

Podoplanin (PDPN)+ FRC are an important stromal component of TLS (figure 2). From neogenesis, FRC form a structural scaffold by assembling into networks and secrete factors to recruit and retain immune cells in the TLS [103]. Another crucial non-immune component of TLS is HEV (figure 2). This specialized vasculature, marked by PNAd, ensures that lymphocytes can traffic between TLS and the blood stream [63].

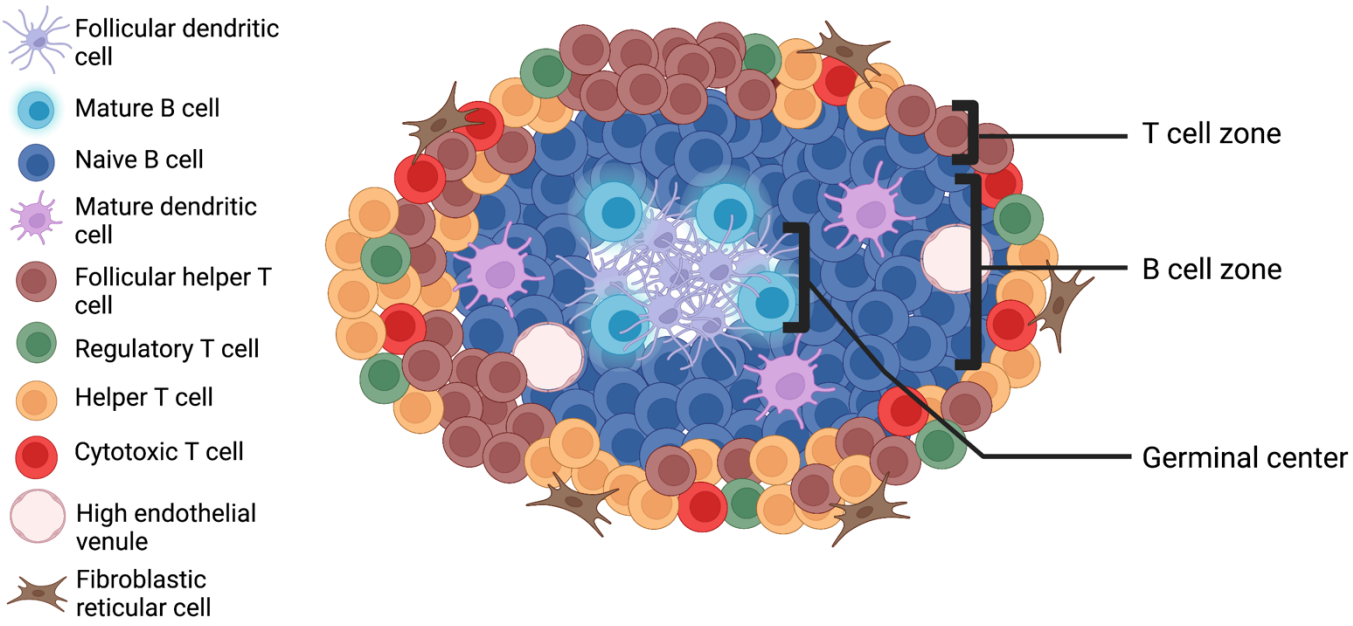

Figure 2: The cellular organization of TLS (figure created with Biorender.com)

1.4.3 Functions

TLS are multi-faceted and should be examined in a context-dependent manner. In auto-immune disease, they were shown to exacerbate progression by mounting B and T cell responses, hence increasing inflammation and tissue damage. Nonetheless, this adaptive immune response is beneficial in controlling infections. Studies also suggest that TLS could carry out regulatory functions that dampen other aspects of the immune system [104].

Firstly, TLS orchestrate the local adaptive immunity. Activated B cells differentiate into plasma cells, secreting tumor-specific antibodies that lead to cell lysis and increased priming of cytotoxic T cells through more efficient DC-mediated antigen uptake [105, 106]. We observe this in TLS of patients with rheumatoid arthritis, where B cells produce antibodies against disease antigens. Evidence of activation, clonal expansion and somatic hypermutation have also been found in TLS of several pathologies, including cancer [94, 107-109]. In fact, a 2022 study of renal cell carcinoma showed that mature TLS in tumors were associated with higher infiltration of plasma cells [110]. TLS can also mount a cellular immune response by both reactivating and priming T cells. In central nervous system (CNS) inflammation, Th17 cells in TLS acquire Tfh features to assist in the GC reaction [67]. In multiple sclerosis, naive T cells become autoreactive to myelin epitopes in CNS-TLS [111]. Early studies in melanoma murine models that lack SLO showed that TLS induction resulted in clonal expansion and increased cytotoxicity of T cells [78, 79]. The most compelling evidence of TLS-orchestrated adaptive immunity comes from a study of iBALT by Moyron-Quiroz *et al*. Mice lacking SLO but retaining iBALT were able to generate robust B and T cell responses to influenza. More shockingly, those mice survived at higher doses of the virus than normal mice, showing superiority to systemic immune responses [86, 87]. This points to the capacity of TLS to independently mount a robust immune response at the local level.

Secondly, TLS can be immunoprotective by harboring regulatory B cells (Breg), Treg, and sequestering effector T cells. Breg are induced in response to high levels of inflammatory cytokines or through B cell receptor (BCR) and Toll-like receptor activation [98]. They secrete immunosuppressive cytokines, such as IL-10, IL-35 and transforming growth factor-β (TGF-β), which dampen T cell response and polarize macrophages towards the pro-tumoral M2 phenotype [98]. Furthermore, Breg can partake in T cell suppression by expressing PD-L1, a phenomenon

that was documented in melanoma patients [112]. In a murine model of atherosclerosis, TLS promote the differentiation of CD4 T cells into Tregs to reduce inflammation [113].Treg are known to promote tumor progression through their immunosuppressive effects. Both Breg and Treg populations were identified in TLS of human breast cancer tissues [114]. Finally, TLS may sequester antigens and effector T cells. This was seen in cases of asthma, where TLS accumulate and isolate Th2 cells, thereby preventing them from inducing airway hyper-responsiveness [104].

1.4.4 Association with cancer outcomes

To date, the majority of studies on TLS in cancer have been exploring their potential as a predictive and prognostic biomarker. Different features of TLS are characterized in those studies, including their presence, location, maturation, density, cellular composition, and chemokine landscape. The methods used in those studies vary as well. Histological assessment methods include hematoxylin and eosin (H&E), immunohistochemistry and immunofluorescent staining with different markers to identify cellular components of TLS. RNA sequencing has also been used in several studies following the discovery of a 12-chemokine (12-CK) signature of TLS [115]. Finally, spatial transcriptomics have been introduced to the field due to their powerful coupling of genomic and spatial information at high resolution.

For the most part, TLS have been associated with positive cancer outcomes. A systematic review of 27 studies including more than 6000 patients found that TLS was associated with increased OS and recurrence free survival (RFS) [116]. This was reported across tumor types, including NSCLC, oral cancers, colorectal cancer, endometrial cancer, and pancreatic cancer [116]. The authors pointed to a positive correlation between TLS and immune infiltration, and a negative correlation with tumor size, which could explain those outcomes [116]. Furthermore, TLS have been linked to long term therapeutic responses to immune checkpoint inhibitors (ICI) and

chemotherapy [117]. In fact, TLS presence has been shown to predict response to ICI in melanoma, soft tissue sarcoma, NSCLC, RCC, pancreatic cancer and bladder cancer [110, 118-122]. In breast cancer, neoadjuvant chemotherapy caused B cells in the TLS to express inducible T-cell costimulator ligand (ICOS-L). This resulted in an increase in the effector to regulatory T cell ratio, improving patient outcomes [123].

Intriguingly, certain characteristics TLS have been associated with negative cancer outcomes. Firstly, location of TLS seems to have an impact. The histological presence and 12-CK score of peritumoral TLS have been associated with shorter OS in hepatocellular carcinoma (HCC) and intrahepatic cholangiocarcinoma, which was the reverse association compared to intratumoral TLS [124-126]. Secondly, TLS maturation matters. In colorectal cancer and HCC, the presence of immature TLS was associated with an increased risk of recurrence [127, 128]. Additionally, non-responding bladder cancer patients to ICI had significantly more immature TLS compared to responders [129]. Finally, the presence of Breg and Treg populations in TLS have been associated with poor outcomes [114, 130]. For example, gastric cancer patients with high IL-10+ Bregs had significantly lower OS thank those with low populations [130].

Chapter 2: Rationale

RT is an attractive alternative to radical cystectomy that allows bladder preservation and spares MIBC patients from the detrimental effects on the quality of life that follow RC. However, up to one in five patients treated with bladder sparing therapy requires a salvage cystectomy, which comes at a high rate of complication and mortality [60].

Although NAC provides an absolute survival benefit of about 5%, only 20-40% of patients downstage at RC [24]. This indicates that the majority of patients are overtreated and left with undesirable toxicities without deriving any benefit.

In this case, biomarkers are an invaluable tool to guide personalized treatment decisions. They can help clinicians optimize patient selection based on predicted therapeutic response. Notably, TLS represent a particularly relevant candidate as they link innate and adaptive immunity in proximity to the tumor. On one hand, they could increase sensitivity to RT and NAC and fine tune the immune response by improving the speed, control, efficiency, and survival of anti-tumoral immunity. On the other hand, they could harbor cells that modulate an immune-suppressive environment.

By characterizing TLS in pre-treatment setting, we can gain insight into the immune landscape of the tumor and assess its likelihood to respond to NAC and RT.

CHAPTER 3: Hypothesis

We hypothesize that TLS are associated with response to RT and NAC in MIBC. We believe that certain characteristic of TLS on patient biopsies could predict and aid in selecting patients that would benefit the most from those therapies.

CHAPTER 4: Aims

This study has two aims:

1. Characterizing TLS in pre-treatment tissues of MIBC patients that underwent RT and NAC and interrogate their association with outcomes.
2. Profiling the TIME in pre-treatment tissues of MIBC patients that underwent RT and examine the association with their TLS profile.

CHAPTER 5: Materials and methods

5.1 Patient cohorts

Two retrospective patient cohorts were used for this study. The RT cohort was composed of 139 consenting patients who were treated with radiation therapy between 2004 and 2021. The NAC cohort was composed of 102 patients who were treated with cisplatin-based neoadjuvant chemotherapy between 2001 and 2021. Pre-treatment tumor biopsies were collected, stored, and used under IRB approval (REB- RI-MUHC #2017-2612). Informed consent was obtained for all patients. Clinical information including age at diagnosis, sex, stage, and outcomes were extracted from the Oasis medical records hospital system. Response to RT was evaluated with urine cytology, white-light cystoscopy, tumor bed biopsy, and cross-sectional imaging within three months after the completion of RT. Response was defined as pathological downstaging, a negative tumor bed biopsy, or a combination of negative urine cytology and normal cystoscopy, along with the absence of any indications of locoregional disease on cross-sectional imaging. Response to NAC was assessed by the pathological stage at RC, where the downstaging or absence of tumor compared to the pre-NAC TURBT was considered as response. Formalin-fixed-paraffin-embedded (FFPE) blocks and diagnostic hematoxylin and eosin (H&E) slides of patients' pre-treatment TURBT were obtained and annotated by a pathologist to identify tumoral, stromal and benign regions. For the RT cohort, tissue microarrays (TMA) were further constructed by punching five cores from selected patient blocks and reassembling into a new FFPE block. Each patient was represented by two tumor cores, two tumor-stroma transition core and one benign tissue core.

5.2 Chromogenic multiplex immunohistochemistry

5µm-thick sections were deparaffinized and rehydrated. Immunohistochemistry (IHC) was performed with the Discovery Ultra instrument from Roche. After antigen retrieval treatment with Tris EDTA for 32 minutes, sections were incubated for 24 minutes at 37°C with primary antibody, followed by 20 minutes of incubation with the secondary antibody and chromogenic detection. The first antibody was then denatured, and the staining steps were repeated for the following antibodies in the sequence. Slides were finally counterstained with hematoxylin/bluing, dehydrated, cleared and cover slipped. Slides were digitally scanned using an Aperio scanner for analysis. In total, four protocols of mIHC were performed. The first one used anti-CD20 (prediluted, Roche) with OmniMap anti-mouse HRP (760-4310, Roche) and ChromoMap DAB detection kit; followed by anti-CD3 (prediluted, Roche) with OmniMap anti-rabbit HRP (760-4311, Roche) and Discovery Purple detection kit (760-229). The second stain used anti-CD23 (1-400, ab27568, Abcam) with OmniMap anti-rabbit HRP and Discovery Purple detection kit, and anti-CD21 (prediluted, Roche) with OmniMap anti-mouse HRP and Discovery Green detection kit (760-271, Roche). The third stain used anti-CD8 (prediluted, Roche) with OmniMap anti-rabbit HRP and ChromoMap DAB detection kit, and anti-Neutrophil Elastase (1-2900, MAB9167, Novus Biologicals) with OmniMap anti-mouse HRP and Discovery Teal detection kit. Finally, a fourplex was performed with anti-CD4 (prediluted, Roche) with OmniMap anti-rabbit HRP and Discovery Purple detection kit, anti-CD20 with OmniMap anti-mouse HRP and ChromoMap DAB detection kit, anti-CD68 (prediluted, Roche) with OmniMap anti-mouse HRP and Discovery Green detection kit, and anti-FoxP3 (1-100, NB100-39002, Novus Biologicals) with OmniMap anti-rabbit HRP and Discovery Teal detection kit.

5.3 TLS characterization

In both cohorts, one representative H&E section from each case was evaluated to detect TLS. In the absence of TLS, slides from other blocks of the same case were screened to find TLS before making a final assessment. Further characterization of the RT cohort was performed through multiplex chromogenic immunohistochemistry by the RI-MUHC Histopathology platform. Blocks with lymphocytic aggregates without a visible germinal center on H&E were double stained by with CD20 and CD3 to confirm the presence of both B and T cells within the aggregate in order to be considered TLS positive. Finally, positive blocks were selected for further dual staining with CD21 and CD23 to assess TLS maturation (figure 3).

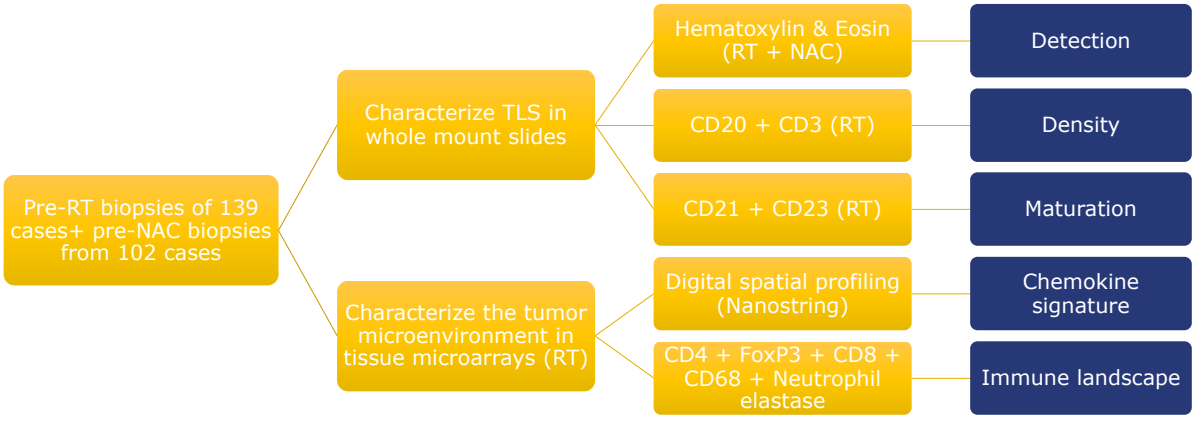

Figure 3: project plan for TLS characterization

5.4 Digital spatial profiling

To obtain a TLS signature, Digital Spatial Profiling from Nanostring Technologies using the GeoMx Whole Transcriptome Atlas was performed. Briefly, immunofluorescent staining was performed on TMA using Pan-cytokeratin and CD45 to identify 300 regions of interest (ROI). *In situ* hybridization with barcoded RNA probes was done, then the oligonucleotide barcodes were cleaved and collected in ROI by subjecting them to ultraviolet light. Finally, the cleaved barcodes

were counted and sequenced. GeoMx DSP Analysis suite was used to perform quality control and normalization.

5.5 Image analysis

Image analysis was performed using Halo version 3.5. TMA were analyzed using the multiplex IHC module, which was optimized to count immune cells (figure 4). In cores containing TLS, a classifier was used to detect and separately count B cells within aggregates as to not bias the results. Due to high morphological heterogeneity, macrophages were detected using the Area quantification module to detect CD68 positive pixels and produce the percentage of positive area. Output was normalized by dividing with the core surface area then averaged for each patient. To quantify density, TLS were manually delineated on the CD20/CD3 sections when available, and the CD21/CD23 or H&E sections otherwise. The sum of TLS surface area was divided by the total tissue surface area for normalization. Maturation was analyzed by manually delineating germinal centers, as well as using the Area quantification module to detect CD21 and CD23 positive pixels within the annotated TLS. The percentage positivity was obtained and summed up for both markers. The average surface areas of TLS and GC were also determined.

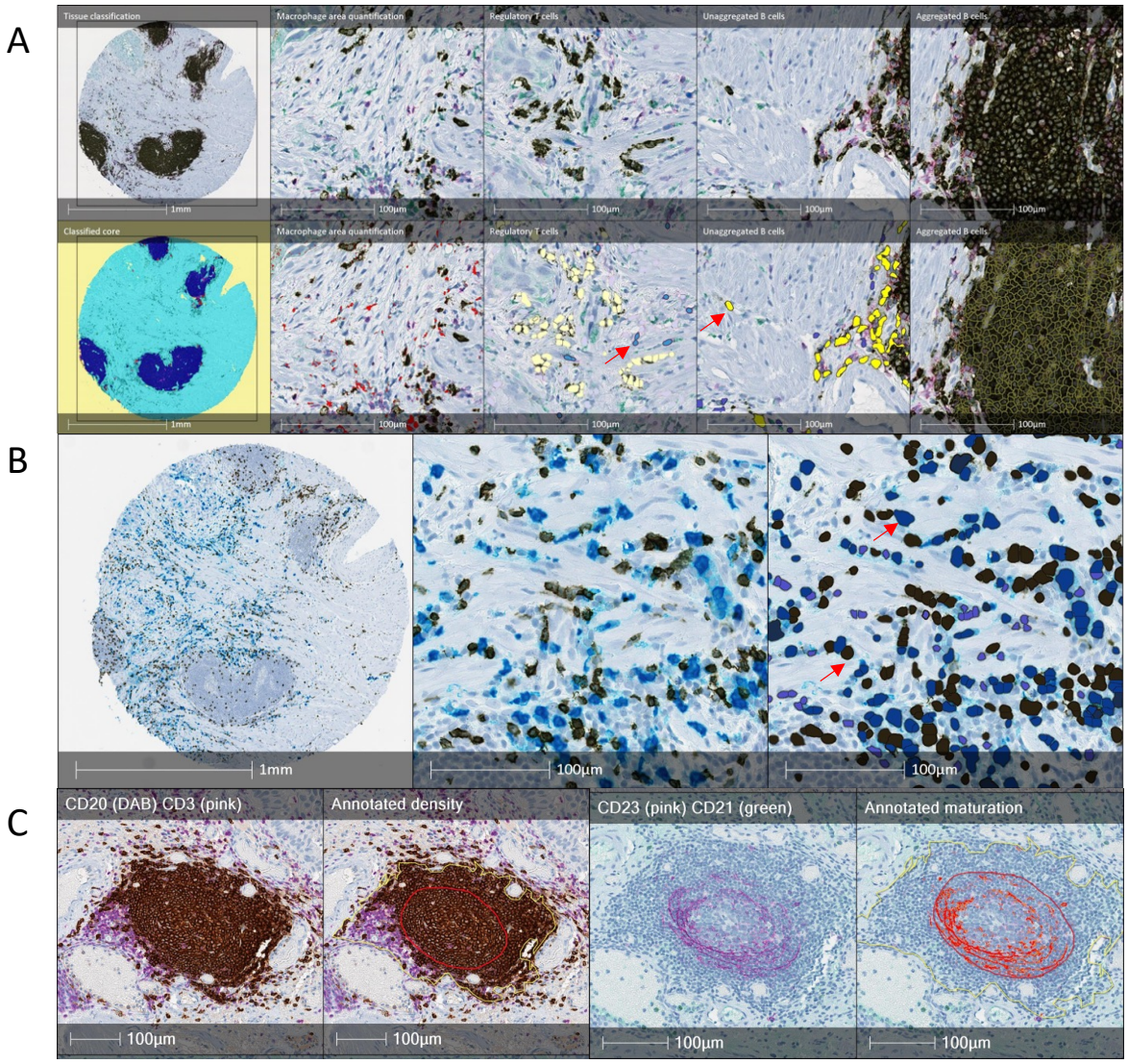

Figure 4: Image analysis on Halo.

A: fourplex IHC staining of TMA core with CD68 (green), FoxP3 (teal)/CD4 (pink), and CD20 (DAB) (top); immune cell quantification using classifier to distinguish areas of B cell aggregation from the rest of the tissue (bottom). B: dual IHC staining of TMA core with CD8 (DAB) and Neutrophil elastase (teal) with quantification. Arrows show single cells counted as output of the algorithm. C: dual IHC staining of TLS density with CD20 (DAB) and CD3 (pink) with annotations (left); dual IHC staining of TLS maturation with CD21 (green) and CD23 (pink) with annotation and analysis of signal positivity (right).

5.6 Statistical analysis

GraphPad version 9 software and RStudio version 4.2.2 were used for statistical analyses and data visualization. The Youden's J-index method was used to find cut-offs that separate patients in two groups based on different TLS characteristics. Difference between responder groups was analyzed using the two-tailed student's t-test or Mann-Whitney test. Survival curves were compared using the log-rank (Mantel-Cox) test. Fisher's exact test was used to assess contingency. Finally, heatmaps were made using the `ComplexHeatmap` R package. The data was log-transformed, scaled, and converted into a matrix. Hierarchical clustering was performed using the "ward.D2" method. A p-value <0.05 was considered statistically significant.

CHAPTER 6: RESULTS

6.1 TLS were highly abundant in muscle invasive bladder cancer

We found aggregates of lymphocytes to be highly abundant and heterogeneous on H&E sections of biopsies. We began by categorizing slides based on the level of certainty of TLS presence (figure 5). Sections that contained TLS with a GC, regardless of size or organization, were considered positive without further staining (figure 5.1-2). Sections that lacked any immune aggregates were considered negative (figure 5.5). Finally, sections with lymphoid aggregates without GC were further stained to evaluate if they were TLS. Additional H&E slides of negative and ambiguous cases were screened to identify any prominent immune aggregate or GC, and the slide with the highest TLS character was retained for further analysis. In the RT cohort, 36% of cases (n=51) had TLS with detectable GC; 54% of cases (n=74) had lymphoid aggregates without GC, and 10% (n=14) were negative for any aggregates. To confirm the identity of lymphocytic aggregates, we proceeded with a dual immunohistochemistry staining with CD20 and CD3 to locate B cells and T cells, respectively. Of the 74 cases, 71 contained both cell types within the immune aggregates, indicating that they are TLS. Overall, TLS were detected in 83% (n=118) of RT cases.

Using the same workflow for the NAC cohort, 62% of cases (n=63) had TLS with GC and were considered positive. Of the remaining 39 cases, 9 cases were negative for TLS, and 30 cases were stained with CD20 and CD3 to evaluate the lymphocytic aggregates observed . Of those, only 4 cases were found negative, amounting to a total of 85% (n= 88) of NAC cases that were positive for TLS.

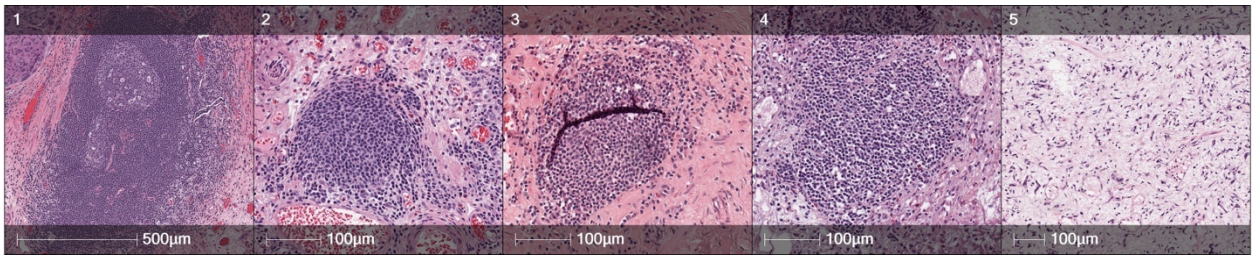

Figure 5: TLS characterization on H&E

H&E staining of whole mount TURBT sections showing TLS (1-2), lymphocytic aggregates (3-4) and absence of any immune cells (5).

6.2 TLS presence was not associated with treatment outcomes and prognosis.

As TLS were detected in most MIBC cases, we investigated whether their presence was associated with better prognosis or response to treatment. To do so, we compared TLS presence among responders and non-responders to RT and NAC (figure 6A). We found that TLS were not associated with response to RT (Fisher's exact test p = 0.797). We also compared cancer specific survival (CSS) and OS between TLS positive and TLS negative cases and found no significant difference in survival (log-rank test p=0.624 for OS and p=0.438 for CSS) (figure 6B-C). Similarly, there was no association between response to NAC and TLS presence (Fisher's exact test p=0.370) (Figure 6A). Although we could observe a trend, there was no significant difference in OS and CSS between the TLS groups (log-rank test p=0.170 for OS and p=0.071 for CSS) (figure 6B-C). Altogether, we concluded that TLS presence was not associated with MIBC treatment response and prognosis.

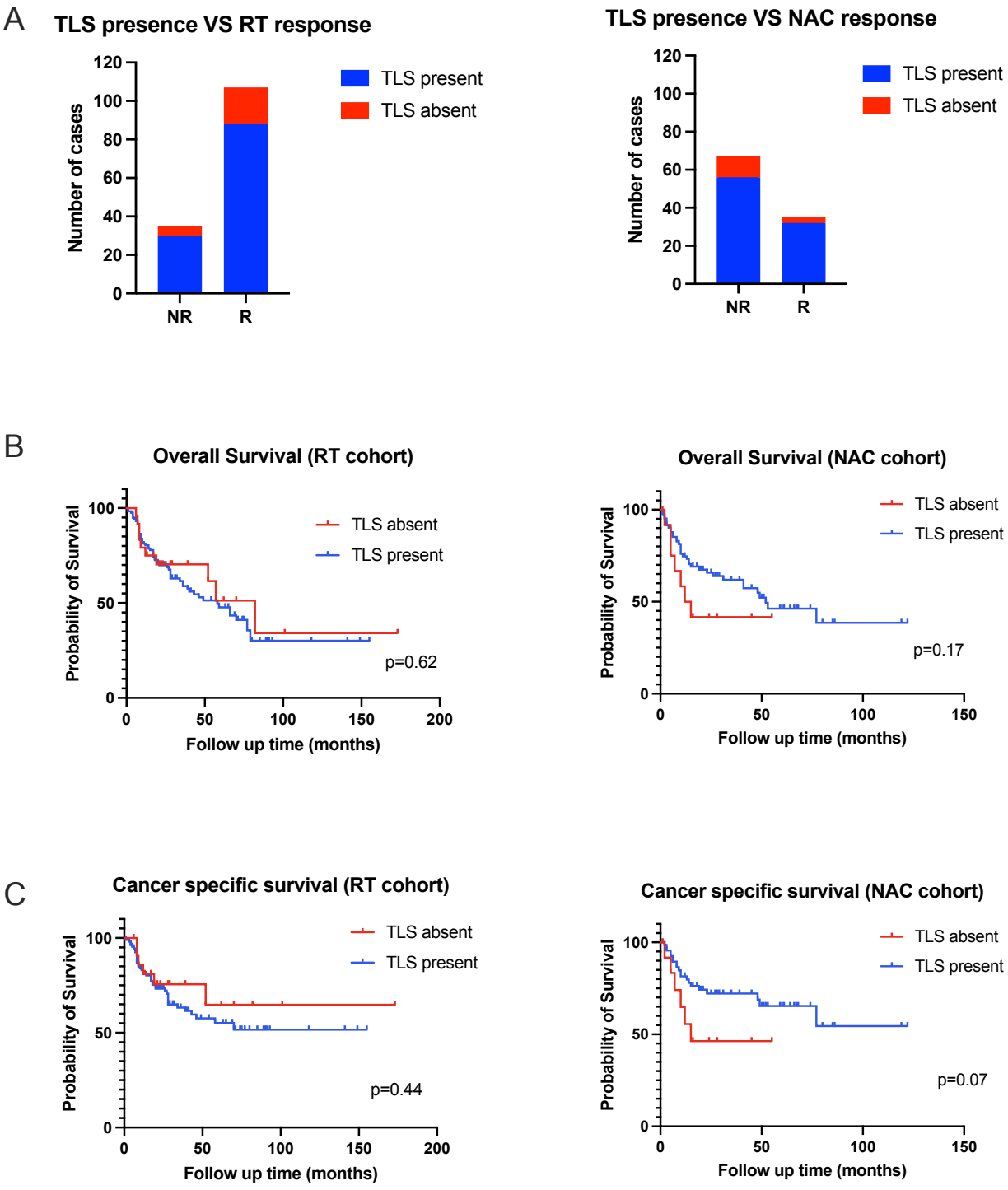

Figure 6: TLS presence was not associated with treatment outcomes and prognosis.

A: TLS presence according to RT response (left) and NAC response (right). R= responders (n=107 for RT, n= 31 for NAC); NR= non responders (n=35 for RT, n= 71 for NAC). Fisher's exact test p = 0.797 for RT and p=0.370 for NAC. B: Kaplan-Meier curves of OS according to TLS presence in RT (left) and NAC (right). Log-rank test p=0.624 for RT and p=0.170 for NAC. C: Kaplan-Meier curves of CSS according to TLS presence in RT (left) and NAC (right). Log-rank test p=0.438 for RT and p=0.071 for NAC.

6.3 Responders to RT have higher TLS density and maturation.

We then sought to distinguish differences in TLS between patients, starting with the quantification of TLS density and maturation. We measured TLS density as the number of TLS divided by the total tissue surface area, as well as the percentage of TLS surface of total tissue surface area [131]. Using both indicators, we found that TLS density was significantly higher among responders compared to non-responders to RT (Mann-Whitney test p=0.01) (figure 7B-C). Maturation was computed in several ways to capture the heterogenic nature of TLS. We considered TLS mature when a GC was present, using CD21 and CD23 to stain for GC FDC, which are established markers in the literature [96]. We defined GC, with the help of a pathologist, as networks of CD21+ and/or CD23+ follicular dendritic cells on mIHC. As such, GC were delineated to find their surface area, number, and average size. Moreover, we analyzed the percentage positivity of CD21 and CD23 signals in the TLS to further compare GC among each other. We first noted a high intra-patient heterogeneity of TLS maturation levels, both in terms of the presence of GC but also in the characteristics of GC. As illustrated in figure 7A, we detected mature TLS with different GC morphologies, staining pattern of CD21 and CD23, and size on the same section. We found that the average size of GC, but not the number or the surface area, was significantly higher among responders compared to non-responders to RT (Mann-Whitney test p=0.026) (figure 7B-C). Interestingly, we found that GC of non-responders are significantly more positive for CD21 compared to complete responders (Mann-Whitney test p=0.04) (figure 7C). No

difference in CD23 signal was detected between the two groups (Mann-Whitney test p=0.84) (figure 7C). Taken together, high TLS density and maturation, marked by GC size, were predictive of response to RT.

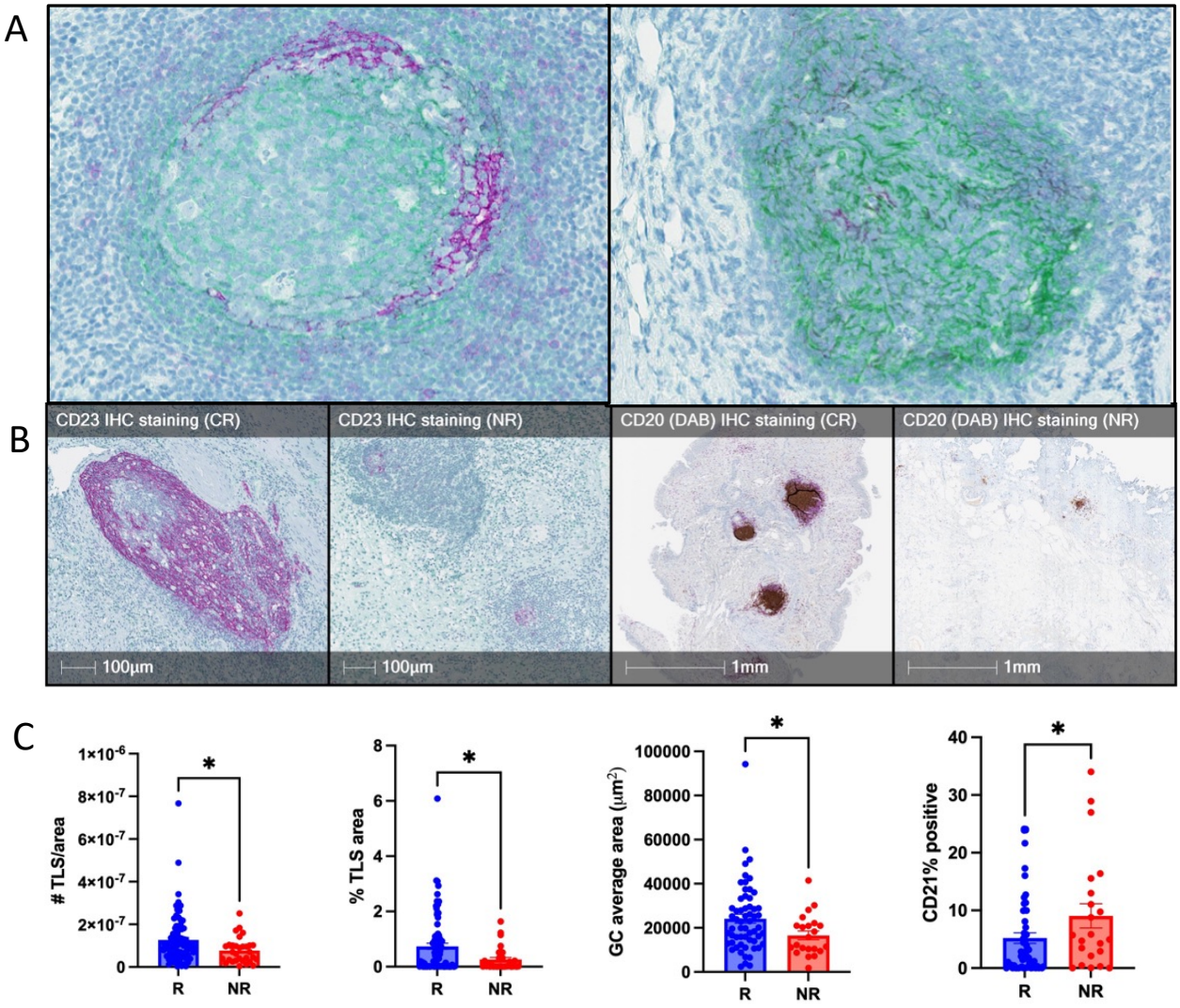

Figure 7: Maturation and density are higher among responders to RT.

A: Heterogeneric morphologies of mature TLS from the same case (dual IHC with CD21 in green and CD23 in pink). B: Representatives images of IHC staining with CD23 (pink) (left) and CD20 (DAB) (right) showing the difference in TLS maturation and density between a responder and a non-responder. C: Comparisons between responders and non-responders of TLS density (Mann-Whitney p=0.01), average GC size (Mann-Whitney p=0.026), and percentage of CD21 positive signal (Mann-Whitney p=0.04).

6.4 Higher TLS density is associated with increased survival.

Next, we compared survival between patients with high and low TLS density and maturation. First, to group patients, a cut-off of 0.57% TLS density (interquartile range= 0.86) was determined using Youden's j-index [132]. When segregating patients into "high-density" and "low-density" groups, we found that patients with high TLS density had a significantly increased OS (Log-rank test p=0.044) and CSS (Log-rank test p=0.034) (figure 8A). The median OS in the high-density group was 77 months, compared to only 36 months in the low-density group. Likewise, patients were divided based on the average GC size using the cut-off of 22800 μm^2 (interquartile range= 17000). We found a similar trend, despite not achieving statistical significance, where patients with a larger average GC size had an increased OS and CSS (Log-rank test p=0.097 and p=0.059, respectively) (figure 8B). Overall, we concluded that high TLS density was associated with prologued survival in MIBC patients.

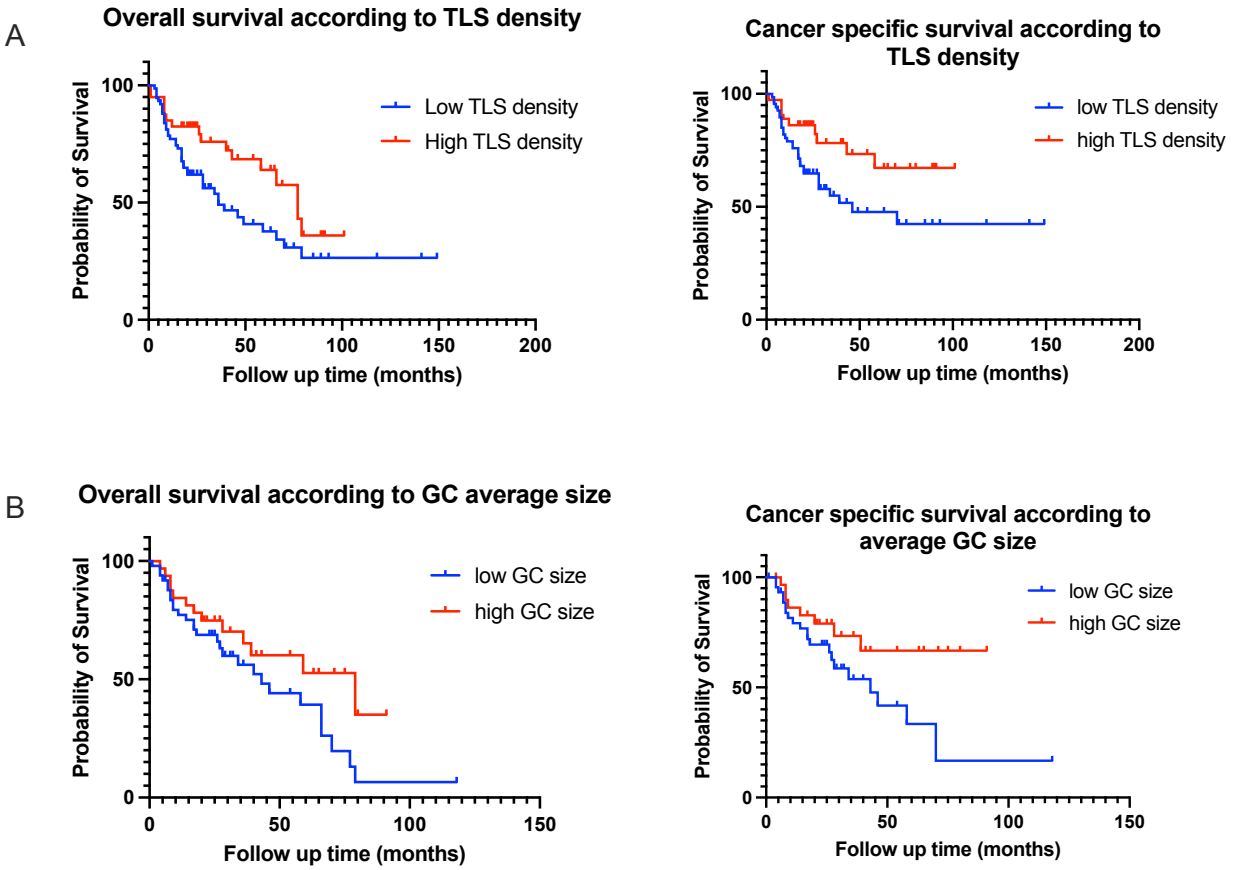

Figure 8: TLS density and maturation are positive prognostic markers.

A: Kaplan-Meier curves of overall survival (left) and cancer specific survival (right) according to TLS density. Cases with TLS density<0.56% were considered in the "Low TLS density" group and cases with density>0.56% were in the "High TLS density" group. Log-rank test p=0.044 for overall survival and p=0.034 for cancer specific survival. B: Kaplan-Meier curves of OS (left) and CSS (right) according to GC average size. Cases with GC average size<22800 μm^2 were considered in the "low GC size" group and cases with GC average size>22800 μm^2 were in the "high GC size" group. Log-rank test p=0.097 for overall survival and p=0.059 for cancer specific survival.

6.5 TLS density is associated with immune infiltration in the TME.

To explore the link between TLS and the surrounding TME, we quantified immune cells in TMA and compared them between TLS density groups using $1.05E^{-1}$ TLS/μm^2 as a cut-off (interquartile range= $9.43E^{-2}$), which was determined by Youden's J-index. We stained for the key

immune players with known roles in the TME : B cells, Treg, macrophages, neutrophils, and cytotoxic T cells. We found that groups with high TLS density had significantly higher B cell and Treg infiltration (Mann-Whitney test $p<0.000$ and $p=0.009$, respectively) (figure 9A). Of note, B cells were quantified outside of any aggregates as to not bias the results (figure 3A). We did not find any difference in infiltration between groups for macrophages ($p=0.210$), neutrophils (0.916), and cytotoxic T cells (0.302). Interestingly, we found a strong positive correlation between regulatory T cells infiltration and TLS density in responders (Pearson's correlation, $r=0.630$, $p=0.043$); whereas TLS density had a negative correlation with cytotoxic T cell infiltration in non-responders (Pearson's correlation, $r=-0.173$, $p=0.029$) (figure 9B). We concluded that TLS density is associated with a certain immune profile, characterized by a high number of B cells and Treg, which is also different among responders and non-responders to RT.

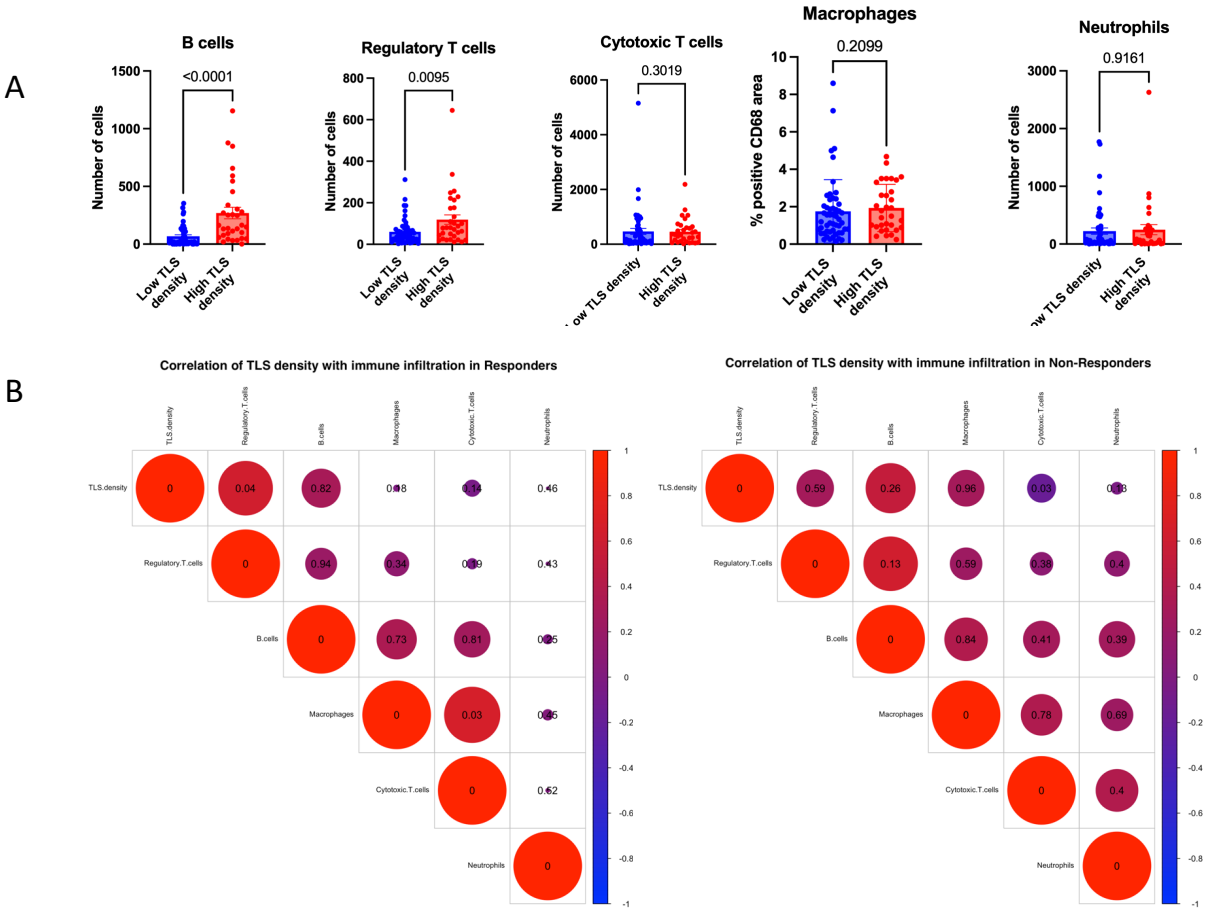

Figure 9: TLS density is associated with immune infiltration.

A: Comparisons between "high TLS density" and "low TLS density" groups of B cell, regulatory T cell, cytotoxic T cell, macrophages, and neutrophil infiltration. Displayed p-values were computed using Mann-Whitney test. B: Correlogram showing correlations between immune cell infiltration and TLS density in responders (left) and non-responders (right). Color of circle indicates Pearson's correlation coefficient (see scale), and size corresponds to the significance. P-values are displayed in each circle.

6.6 TLS 12-chemokine signature is associated with response to RT.

Finally, we sought to examine the previously described TLS 12-chemokine signature and its association with response to RT [115]. From the whole-transcriptome analysis data, we extracted the following genes: *CCL2, CCL3, CCL4, CCL5, CCL8, CCL18, CCL19, CCL21, CXCL9, CXCL10, CXCL11,* and *CXCL13*. We then separated the expression in Pan-cytokeratin (PanCK) + regions and PanCK- regions to separately analyze data in the tumor and stroma, respectively. Through unsupervised hierarchical clustering, we identified a cluster of cases with low TLS signature in the stroma that is highly enriched in non-responders (figure 10). We also found a small cluster of patients with high TLS signature expression in the tumor that exclusively contains responders (figure 10). Taken together, our results indicate that expression of the TLS chemokines is associated with response to RT.

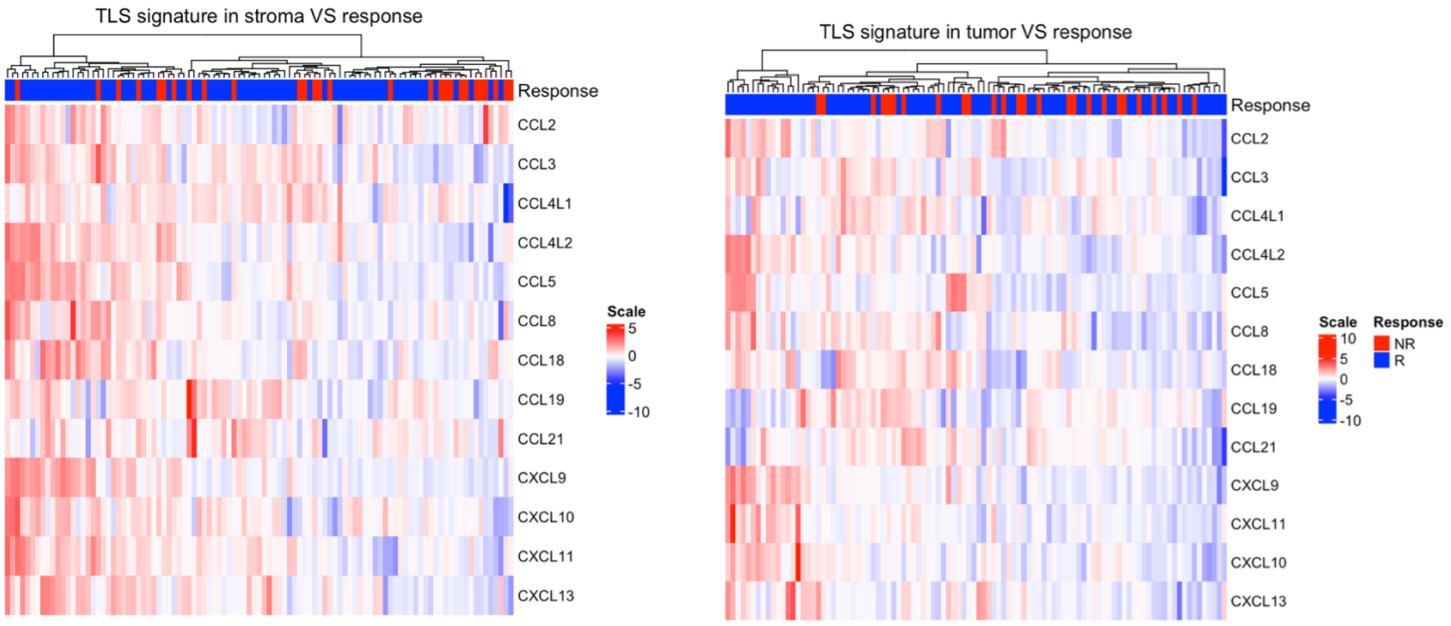

Figure 10: TLS signature is associated with response.

Heatmaps showing the 12-chemokine signature of TLS annotated with RT response. Hierarchical clustering was performed using the "ward.D2" method on R.

CHAPTER 7: DISCUSSION

TLS have emerged as crucial players in the immune response against tumors, while also serving as potential indicators of prognosis and treatment response. Despite extensive research, many mysteries surrounding TLS persist. For instance, the specific interactions between NAC, RT and TLS are still unknown. Furthermore, the mechanisms governing TLS-mediated immune regulation and intercellular interactions, particularly between B cells and T cells, remain elusive. Consequently, there is an immediate and pressing need to comprehensively explore the role of TLS in malignancies.

In this study, we investigated TLS in the context of local response to MIBC treatments, particularly NAC and RT, using TURBT samples. We found that TLS presence alone does not predict response to either treatment modality (figure 6). We then chose the RT cohort to further profile TLS, characterizing their density, maturation, chemokine signature, and the immune microenvironment. Density and maturation of TLS were found to be higher among responders to RT and were predictors of increased survival (figure 7-8) . Furthermore, we found that the 12-CK signature was highly expressed in the stroma of a cluster of responders to RT, and poorly expressed in the tumors of non-responders (figure 9). Finally, we found that high TLS density was correlated with increased immune infiltration (figure 10).

Research of TLS in MIBC is still scarce and limited in cohort size. In our cohorts, we found TLS in about 85% of patients, which is higher than the 50-75% reported in other studies[122, 131, 133, 134]. The most likely explanation for this discrepancy is the methodology employed for TLS screening and considerations when defining TLS. In contrast to other studies that typically assess a single representative slide per patient, we meticulously evaluated every available H&E slide prior to confirming the absence of TLS. It is important to note that a significant portion of TLS is

primarily located in the lamina propria. Consequently, if a slide solely consisted of epithelial tumor tissue, it would generally result in the absence of observable TLS. Moreover, variations in techniques used for TLS assessment contribute to the diversity of results. Some studies employ histological techniques like H&E staining, while others use IHC/IF, or RNA sequencing [131, 134]. The latter studies rely on surrogate markers such as CXCL13 or the 12-CK signature as indicators of TLS presence [115]. Finally, there is a lack of consensus regarding the definition of TLS. Some studies consider any aggregates of B cells and T cells as early TLS [133]. Others impose stringent criteria, considering only TLS structures with follicular morphology and well-defined T cell and B cell compartments [134]. In this study, we considered any aggregates of B cells and T cells as TLS using a combination of H&E and CD20/CD3 mIHC staining. To complement our characterization, we also used the 12-CK signature extracted from DSP data. This approach allowed us to capture the most accurate and complete picture of the TLS profile of each patient and ensured that we explore every TLS characteristic that might be associated with treatment response.

From a biological perspective, the high prevalence of patients presenting with TLS in the bladder is indeed sensible. Given that the bladder is a mucosal organ, it is susceptible to lymphocyte infiltration. In fact, TLS formation occurs in all bladder pathologies, including cystitis cystica, bladder pain syndrome/Hunner's lesion interstitial cystitis, follicular cystitis, and cancer [135]. Moreover, the impact of age is noteworthy, as it contributes to increased inflammation. Studies in mice have reported the development of TLS in the normal bladder as age progresses [72]. Considering that older age is the primary risk factor for MIBC, and that cancer is described as a “wound that never heals”, it is not surprising that it also drives TLS formation. Exploring potential functional differences between TLS induced by aging and TLS induced by tumors could

be an intriguing avenue for future *in vivo* studies. Understanding whether these two types of TLS exhibit distinct characteristics would provide valuable insights into their respective roles and mechanisms.

The association between TLS and outcomes has yielded varying results in different studies. While some suggest that the presence of TLS is associated with increased survival in MIBC, others do not find such an association [115, 131, 136]. Our analysis is consistent with the latter observation, as we discovered that the presence of TLS alone is not prognostic. To the best of our knowledge, this is the first study to link TLS characteristics with response to RT in any cancer setting and to NAC in MIBC. In breast cancer, TLS characteristics and 12-CK scores were associated with NAC response [76, 137]. In esophageal squamous cell carcinoma, mature TLS were predictive of response and increased relapse free survival [138]. Intriguingly, contradictory results are reported in NSCLC, where certain studies find a positive association of TLS maturation and density with NAC response, and others do not [139, 140]. Our results are probably a consequence of TLS abundance in MIBC as we discussed previously and pointed us to further characterize them and the TME to draw out differences between response groups.

We found that TLS density was both a positive prognostic biomarker and predictive of response to RT. This is in agreement with another study in MIBC that found density and not presence of TLS to be prognostic using The Cancer Genome Atlas and IMvigor210 cohorts [131]. We assessed density through both the quantification of TLS numbers and their surface area normalized by the total tissue surface area, although density is typically measured through the former way. Our choice was driven by a recent paper on colorectal cancer, which showcased a 3D tissue reconstruction that revealing the formation of large TLS networks that were interconnected with Peyer's patches [141]. Accordingly, in histological sections, it is sometimes difficult to

distinguish the exact boundaries of individual TLS. By employing these two approaches, we aimed to quantify TLS as accurately as possible. Immunologically, TLS density may indicate that there's a quantifiable threshold beyond which the scale is tipped towards an anti-tumoral response. Since the observed densities mainly comprise B cells, as shown by CD20 staining, it is possible that humoral immunity plays a role in facilitating RT-induced ICD, such as antibody-dependent cytotoxicity. Moreover, these B cells could also serve as antigen-presenting cells, contributing to the engagement of surrounding T cells in the immune response. Considering that the field of cancer immunology has predominantly focused on T cell-related mechanisms, a deeper exploration of B cell biology and their impact within the context of cancer is needed.

TLS maturation was previously shown to be predictive of response to immune checkpoint inhibitors in MIBC [122]. Within our cohort, GC exhibited considerable heterogeneity in staining patterns and size, both within individual patients and across different patients. Notably, we found GC that only expressed CD23 without CD21, a phenomenon not previously documented in the literature. Given our aim to capture the intra-patient heterogeneity, we opted against utilizing a qualitative approach that categorized cases as "primary follicle-like" or "secondary follicle-like," which are stages of maturation. Instead, we measured the size of GC and quantified the signals of CD21 and CD23. Interestingly, we found that the density of GC did not have a significant impact, but rather the average size of GC was notably larger among responders to RT. We also observed a trend where larger GC on average was associated with increased survival, despite not achieving statistical significance. Those observations align with the biology of SLO, where active GC tend to grow in size and subsequently contract at the end of an infection. Based on these findings, we can imagine that tumors harboring larger GCs possess a more immunologically active TME, influenced by the activity of GCs in antigen presentation and B cell activation processes. Our most

conflicting finding was that CD21 was more abundantly expressed in the follicles of non-responders to RT. CD21 binds iC3b and C3d which are attached to immune complexes, hence its role in antigen presentation on FDC. In SLO, CD21+ FDC are found in the primary foci, constituting the first phase of the humoral response to generate short-lived plasmablasts [142]. We could not find any evidence in the literature on dysfunction of CD21-mediated antigen presentation, but we hypothesize that it could be a mechanism that contributes to non-response to RT. Further evaluation of this pathway and characterization of tissue with increased CD21+FDC is needed to better understand this observation.

Unsurprisingly, we found an association between immune infiltration and TLS density. Due to the abundant production of CXCL13 in TLS during its formation and maintenance, we anticipate that a high concentration of CXCL13 would attract a greater number of B cells to the TME [75]. Although Treg are acknowledged for their immunosuppressive role in cancer, they also play a critical role in maintaining self-tolerance during the humoral response by inhibiting autoreactive B cells [143]. Therefore, the increased infiltration of Tregs might simply be a consequence of a more robust humoral response that requires additional regulation. In non-responders, a negative correlation was observed between CD8+ T cells and TLS density. As discussed in the introduction, TLS could seclude effector T cells to prevent further tissue damage, which may be the underlying mechanism at play. This would have a direct negative consequence on ICD and T cell mediated cytotoxicity of tumor cells which could contribute to non-response to RT. It is important to remember that the directionality of this association has not yet been established, i.e., we still have yet to understand whether a highly infiltrated TME leads to the formation of more TLS, or whether the formation of TLS increases immune infiltration of the TME.

Finally, we successfully categorized patients into clusters based on their expression of the 12-CK signature. Previously, the 12-CK has been highly associated with mature TLS in MIBC and was found to correlate with increased survival. However, its expression had the largest range between all other studied cancer types[115]. Typically, 12-CK score is extracted from bulk RNA-seq data. Since our gene expression data was obtained through DSP, this could be considered a limitation as the amount of detected RNA is decreased. Nevertheless, DSP allowed us to differentiate between expression in the stroma and the tumor, which is the strength that bulk-RNA sequencing lacks. Unsupervised clustering revealed that the cluster exhibiting the highest expression of chemokines in the stroma consisted entirely of responders. In contrast, the cluster displaying the lowest expression of chemokines in the tumor was enriched with non-responders. This observation aligns with our previous result, which demonstrated that responders had a higher density of TLS, as TLS primarily form in the lamina propria and are expected to exhibit increased chemokine expression with higher density. It was interesting to observe that low expression of 12-CK in the tumor, rather than the stroma, was associated with non-response. The diminished expression of chemokines likely indicates reduced immune activity and TLS presence within the tumor, leading to a lower occurrence of immunogenic cell death (ICD) and consequently resulting in non-response.

Our findings suggest that TLS hold predictive value in the context of RT in MIBC. TLS represent a promising area of research, necessitating a comprehensive understanding of their formation, cellular components, and their role in mediating therapeutic responses. Gaining a deeper understanding of these aspects could potentially uncover strategies to enhance or diminish TLS formation, modify their composition, or enhance their functionality to achieve more favorable treatment outcomes. Studies like ours, which identify specific characteristics of TLS and establish

their association with therapy response, play a crucial role in guiding therapeutic interventions. Not only did we identify a selection biomarker to guide personalized treatment decision, but we also narrowed down the relevant aspects of TLS biology to target for therapeutic benefit. In the context of our study, it is conceivable that promoting increased TLS formation (higher density) could potentially enhance the response to RT, for instance.

CHAPTER 8: CONCLUSION

In this study, we established an association between TLS characteristics and response to RT in the context of MIBC. We also investigated the presence of TLS in NAC pre-treatment biopsies and found no correlation with response. In the context of RT, TLS density, maturation, and chemokine signature were higher among responders. We also found a correlation between TLS and immune infiltration, which hints at a crosstalk between them and the TME. Interestingly, in non-responders, TLS were negatively correlated with CD8+ cytotoxic T cells. Depending on their functions and cellular compositions, TLS could be drivers of response or non-response to treatment. Overall, our findings could guide the selection of patients that could benefit the most from RT to avoid downstream recurrence. Further investigations on the mechanisms governing TLS formation and their interplay with the TME are needed to identify therapeutic targets of TLS modulation.

References:

1. Shermadou, E.S., S. Rahman, and S.W. Leslie, *Anatomy, Abdomen and Pelvis: Bladder*, in *StatPearls*. 2023: Treasure Island (FL).
2. Saginala, K., et al., *Epidemiology of Bladder Cancer.* Med Sci (Basel), 2020. **8**(1).
3. Stringer, L., et al., *Assessing geographic and industry-related trends in bladder cancer in Ontario: A population-based study.* Can Urol Assoc J, 2022. **16**(2): p. E82-e87.
4. Marks, P., et al., *Female with bladder cancer: what and why is there a difference?* Transl Androl Urol, 2016. **5**(5): p. 668-682.
5. Sung, H., et al., *Global Cancer Statistics 2020: GLOBOCAN Estimates of Incidence and Mortality Worldwide for 36 Cancers in 185 Countries.* CA Cancer J Clin, 2021. **71**(3): p. 209-249.
6. Lenis, A.T., et al., *Bladder Cancer: A Review.* JAMA, 2020. **324**(19): p. 1980-1991.
7. Mossanen, M. and J.L. Gore, *The burden of bladder cancer care: direct and indirect costs.* Curr Opin Urol, 2014. **24**(5): p. 487-91.
8. Li, Y., et al., *Frontiers in Bladder Cancer Genomic Research.* Frontiers in Oncology, 2021. **11**.
9. Zhang, X. and Y. Zhang, *Bladder Cancer and Genetic Mutations.* Cell Biochemistry and Biophysics, 2015. **73**(1): p. 65-69.
10. Cohn, J.A., et al., *Sex disparities in diagnosis of bladder cancer after initial presentation with hematuria: a nationwide claims-based investigation.* Cancer, 2014. **120**(4): p. 555-61.
11. Jacobs, B.L., C.T. Lee, and J.E. Montie, *Bladder Cancer in 2010: How Far have We Come?* CA: A Cancer Journal for Clinicians, 2010. **60**(4): p. 244-272.
12. Compérat, E.M., et al., *Grading of Urothelial Carcinoma and The New "World Health Organisation Classification of Tumours of the Urinary System and Male Genital Organs 2016".* European Urology Focus, 2019. **5**(3): p. 457-466.
13. Cortazar, P., et al., *Pathological complete response and long-term clinical benefit in breast cancer: the CTNeoBC pooled analysis.* Lancet, 2014. **384**(9938): p. 164-72.
14. Springfeld, C., et al., *Neoadjuvant therapy for pancreatic cancer.* Nature Reviews Clinical Oncology, 2023. **20**(5): p. 318-337.
15. Zhu, Z., Y.B. Gong, and H.M. Xu, *Neoadjuvant therapy strategies for advanced gastric cancer: Current innovations and future challenges.* Chronic Dis Transl Med, 2020. **6**(3): p. 147-157.
16. Scher, H.I., et al., *Neoadjuvant M-VAC (methotrexate, vinblastine, doxorubicin and cisplatin) effect on the primary bladder lesion.* J Urol, 1988. **139**(3): p. 470-4.
17. Vale, C.L., *Neoadjuvant Chemotherapy in Invasive Bladder Cancer: Update of a Systematic Review and Meta-Analysis of Individual Patient Data: Advanced Bladder Cancer (ABC) Meta-analysis Collaboration.* European Urology, 2005. **48**(2): p. 202-206.
18. Grossman, H.B., et al., *Neoadjuvant Chemotherapy plus Cystectomy Compared with Cystectomy Alone for Locally Advanced Bladder Cancer.* New England Journal of Medicine, 2003. **349**(9): p. 859-866.
19. *MVAC chemotherapy for urothelial carcinoma*. 2023 [cited 2023; Available from: https://www.uptodate.com/contents/image?imageKey=ONC%2F64950.
20. Maase, H.v.d., et al., *Gemcitabine and Cisplatin Versus Methotrexate, Vinblastine, Doxorubicin, and Cisplatin in Advanced or Metastatic Bladder Cancer: Results of a*

Large, Randomized, Multinational, Multicenter, Phase III Study. Journal of Clinical Oncology, 2000. **18**(17): p. 3068-3077.
21. Link, H., *Current state and future opportunities in granulocyte colony-stimulating factor (G-CSF).* Support Care Cancer, 2022. **30**(9): p. 7067-7077.
22. Choueiri, T.K., et al., *Neoadjuvant dose-dense methotrexate, vinblastine, doxorubicin, and cisplatin with pegfilgrastim support in muscle-invasive urothelial cancer: pathologic, radiologic, and biomarker correlates.* J Clin Oncol, 2014. **32**(18): p. 1889-94.
23. Plimack, E.R., et al., *Accelerated methotrexate, vinblastine, doxorubicin, and cisplatin is safe, effective, and efficient neoadjuvant treatment for muscle-invasive bladder cancer: results of a multicenter phase II study with molecular correlates of response and toxicity.* J Clin Oncol, 2014. **32**(18): p. 1895-901.
24. Zargar, H., et al., *Multicenter assessment of neoadjuvant chemotherapy for muscle-invasive bladder cancer.* Eur Urol, 2015. **67**(2): p. 241-9.
25. Pfister, C., et al., *Dose-Dense Methotrexate, Vinblastine, Doxorubicin, and Cisplatin or Gemcitabine and Cisplatin as Perioperative Chemotherapy for Patients With Nonmetastatic Muscle-Invasive Bladder Cancer: Results of the GETUG-AFU V05 VESPER Trial.* Journal of Clinical Oncology, 2022. **40**(18): p. 2013-2022.
26. Lee, Y.S., et al., *Gemcitabine–cisplatin versus MVAC chemotherapy for urothelial carcinoma: a nationwide cohort study.* Scientific Reports, 2023. **13**(1): p. 3682.
27. Patel, V.G., W.K. Oh, and M.D. Galsky, *Treatment of muscle-invasive and advanced bladder cancer in 2020.* CA: A Cancer Journal for Clinicians, 2020. **70**(5): p. 404-423.
28. Baskar, R., et al., *Biological response of cancer cells to radiation treatment.* Front Mol Biosci, 2014. **1**: p. 24.
29. Baskar, R., et al., *Cancer and radiation therapy: current advances and future directions.* Int J Med Sci, 2012. **9**(3): p. 193-9.
30. Huncharek, M., J. Muscat, and J.F. Geschwind, *Planned preoperative radiation therapy in muscle invasive bladder cancer; results of a meta-analysis.* Anticancer Res, 1998. **18**(3b): p. 1931-4.
31. Tholomier, C., L. Souhami, and W. Kassouf, *Bladder-sparing protocols in the treatment of muscle-invasive bladder cancer.* Translational Andrology and Urology, 2020. **9**(6): p. 2920-2937.
32. Huddart, R.A., et al., *LIFE AND DEATH OF SPARE (SELECTIVE BLADDER PRESERVATION AGAINST RADICAL EXCISION): REFLECTIONS ON WHY THE SPARE TRIAL CLOSED.* BJU International, 2010. **106**(6): p. 753-755.
33. Lobo, N., et al., *Landmarks in the treatment of muscle-invasive bladder cancer.* Nature reviews. Urology, 2017. **14**(9): p. 565-574.
34. Zlotta, A.R., et al., *Radical cystectomy versus trimodality therapy for muscle-invasive bladder cancer: a multi-institutional propensity score matched and weighted analysis.* The Lancet Oncology, 2023. **24**(6): p. 669-681.
35. Ricci, M.S. and W.X. Zong, *Chemotherapeutic approaches for targeting cell death pathways.* Oncologist, 2006. **11**(4): p. 342-57.
36. Dhuriya, Y.K. and D. Sharma, *Necroptosis: a regulated inflammatory mode of cell death.* Journal of Neuroinflammation, 2018. **15**(1): p. 199.
37. Dasari, S. and P.B. Tchounwou, *Cisplatin in cancer therapy: molecular mechanisms of action.* Eur J Pharmacol, 2014. **740**: p. 364-78.

38. Sancho-Martínez, S.M., et al., *Necrotic Concentrations of Cisplatin Activate the Apoptotic Machinery but Inhibit Effector Caspases and Interfere with the Execution of Apoptosis.* Toxicological Sciences, 2011. **122**(1): p. 73-85.
39. de Sousa Cavalcante, L. and G. Monteiro, *Gemcitabine: Metabolism and molecular mechanisms of action, sensitivity and chemoresistance in pancreatic cancer.* European Journal of Pharmacology, 2014. **741**: p. 8-16.
40. Pardo, R., et al., *Gemcitabine Induces the VMP1-Mediated Autophagy Pathway to Promote Apoptotic Death in Human Pancreatic Cancer Cells.* Pancreatology, 2010. **10**(1): p. 19-26.
41. Koźmiński, P., et al., *Overview of Dual-Acting Drug Methotrexate in Different Neurological Diseases, Autoimmune Pathologies and Cancers.* Int J Mol Sci, 2020. **21**(10).
42. Meredith, A.-M. and C.R. Dass, *Increasing role of the cancer chemotherapeutic doxorubicin in cellular metabolism.* Journal of Pharmacy and Pharmacology, 2016. **68**(6): p. 729-741.
43. Thorn, C.F., et al., *Doxorubicin pathways: pharmacodynamics and adverse effects.* Pharmacogenetics and Genomics, 2011. **21**(7).
44. Dhyani, P., et al., *Anticancer potential of alkaloids: a key emphasis to colchicine, vinblastine, vincristine, vindesine, vinorelbine and vincamine.* Cancer Cell International, 2022. **22**(1): p. 206.
45. Kim, B.M., et al., *Therapeutic Implications for Overcoming Radiation Resistance in Cancer Therapy.* Int J Mol Sci, 2015. **16**(11): p. 26880-913.
46. Adjemian, S., et al., *Ionizing radiation results in a mixture of cellular outcomes including mitotic catastrophe, senescence, methuosis, and iron-dependent cell death.* Cell Death & Disease, 2020. **11**(11): p. 1003.
47. Hanahan, D. and R.A. Weinberg, *Hallmarks of cancer: the next generation.* Cell, 2011. **144**(5): p. 646-74.
48. Kroemer, G., et al., *Immunogenic cell stress and death.* Nature Immunology, 2022. **23**(4): p. 487-500.
49. Vanmeerbeek, I., et al., *Trial watch: chemotherapy-induced immunogenic cell death in immuno-oncology.* OncoImmunology, 2020. **9**(1): p. 1703449.
50. Zhu, M., et al., *Immunogenic Cell Death Induction by Ionizing Radiation.* Frontiers in Immunology, 2021. **12**.
51. Fabian, K.P., B. Wolfson, and J.W. Hodge, *From Immunogenic Cell Death to Immunogenic Modulation: Select Chemotherapy Regimens Induce a Spectrum of Immune-Enhancing Activities in the Tumor Microenvironment.* Frontiers in Oncology, 2021. **11**.
52. Sherif, A., M. Winerdal, and O. Winqvist, *Immune Responses to Neoadjuvant Chemotherapy in Muscle Invasive Bladder Cancer.* Bladder Cancer, 2018. **4**(1): p. 1-7.
53. Boustani, J., et al., *The 6th R of Radiobiology: Reactivation of Anti-Tumor Immune Response.* Cancers (Basel), 2019. **11**(6).
54. Ngwa, W., et al., *Using immunotherapy to boost the abscopal effect.* Nature Reviews Cancer, 2018. **18**(5): p. 313-322.
55. Ishiyama, Y., et al., *Possible abscopal effect in urothelial carcinoma of the upper urinary tract after treatment with immune checkpoint inhibitors.* IJU Case Rep, 2020. **3**(1): p. 25-27.

56. Craig, D.J., et al., *Systemic benefit of radiation therapy via abscopal effect.* Frontiers in Oncology, 2022. **12**.
57. Rompré-Brodeur, A., et al., *PD-1/PD-L1 Immune Checkpoint Inhibition with Radiation in Bladder Cancer: In Situ and Abscopal Effects.* Molecular Cancer Therapeutics, 2020. **19**(1): p. 211-220.
58. Liu, Y.-P., et al., *Molecular mechanisms of chemo- and radiotherapy resistance and the potential implications for cancer treatment.* MedComm, 2021. **2**(3): p. 315-340.
59. Wernyj, R.P. and P.J. Morin, *Molecular mechanisms of platinum resistance: still searching for the Achilles' heel.* Drug Resist Updat, 2004. **7**(4-5): p. 227-32.
60. Schuettfort, V.M., et al., *Incidence and outcome of salvage cystectomy after bladder sparing therapy for muscle invasive bladder cancer: a systematic review and meta-analysis.* World J Urol, 2021. **39**(6): p. 1757-1768.
61. Barker, H.E., et al., *The tumour microenvironment after radiotherapy: mechanisms of resistance and recurrence.* Nat Rev Cancer, 2015. **15**(7): p. 409-25.
62. Dieu-Nosjean, M.-C., et al., *Long-Term Survival for Patients With Non–Small-Cell Lung Cancer With Intratumoral Lymphoid Structures.* Journal of Clinical Oncology, 2008. **26**(27): p. 4410-4417.
63. Ager, A., *High Endothelial Venules and Other Blood Vessels: Critical Regulators of Lymphoid Organ Development and Function.* Frontiers in Immunology, 2017. **8**.
64. van de Pavert, S.A. and R.E. Mebius, *New insights into the development of lymphoid tissues.* Nat Rev Immunol, 2010. **10**(9): p. 664-74.
65. Carrega, P., et al., *NCR(+)ILC3 concentrate in human lung cancer and associate with intratumoral lymphoid structures.* Nat Commun, 2015. **6**: p. 8280.
66. Deteix, C., et al., *Intragraft Th17 infiltrate promotes lymphoid neogenesis and hastens clinical chronic rejection.* J Immunol, 2010. **184**(9): p. 5344-51.
67. Peters, A., et al., *Th17 cells induce ectopic lymphoid follicles in central nervous system tissue inflammation.* Immunity, 2011. **35**(6): p. 986-96.
68. Lochner, M., et al., *Microbiota-induced tertiary lymphoid tissues aggravate inflammatory disease in the absence of RORγt and LTi cells.* Journal of Experimental Medicine, 2010. **208**(1): p. 125-134.
69. Marinkovic, T., et al., *Interaction of mature CD3+CD4+ T cells with dendritic cells triggers the development of tertiary lymphoid structures in the thyroid.* J Clin Invest, 2006. **116**(10): p. 2622-32.
70. Rangel-Moreno, J., et al., *The development of inducible bronchus-associated lymphoid tissue depends on IL-17.* Nat Immunol, 2011. **12**(7): p. 639-46.
71. Guedj, K., et al., *M1 macrophages act as LTβR-independent lymphoid tissue inducer cells during atherosclerosis-related lymphoid neogenesis.* Cardiovascular Research, 2013. **101**(3): p. 434-443.
72. Ligon, M.M., et al., *Single cell and tissue-transcriptomic analysis of murine bladders reveals age- and TNFα-dependent but microbiota-independent tertiary lymphoid tissue formation.* Mucosal Immunol, 2020. **13**(6): p. 908-918.
73. Peske, J.D., et al., *Effector lymphocyte-induced lymph node-like vasculature enables naive T-cell entry into tumours and enhanced anti-tumour immunity.* Nature Communications, 2015. **6**(1): p. 7114.
74. Rodriguez, A.B., et al., *Immune mechanisms orchestrate tertiary lymphoid structures in tumors via cancer-associated fibroblasts.* Cell Rep, 2021. **36**(3): p. 109422.

75. Yang, M., et al., *CXCL13 shapes immunoactive tumor microenvironment and enhances the efficacy of PD-1 checkpoint blockade in high-grade serous ovarian cancer.* J Immunother Cancer, 2021. **9**(1).
76. Gu-Trantien, C., et al., *CD4+ follicular helper T cell infiltration predicts breast cancer survival.* J Clin Invest, 2013. **123**(7): p. 2873-92.
77. Thommen, D.S., et al., *A transcriptionally and functionally distinct PD-1(+) CD8(+) T cell pool with predictive potential in non-small-cell lung cancer treated with PD-1 blockade.* Nat Med, 2018. **24**(7): p. 994-1004.
78. Schrama, D., et al., *Targeting of lymphotoxin-alpha to the tumor elicits an efficient immune response associated with induction of peripheral lymphoid-like tissue.* Immunity, 2001. **14**(2): p. 111-21.
79. Schrama, D., et al., *Immunological tumor destruction in a murine melanoma model by targeted LTalpha independent of secondary lymphoid tissue.* Cancer Immunol Immunother, 2008. **57**(1): p. 85-95.
80. Martinet, L., et al., *High endothelial venule blood vessels for tumor-infiltrating lymphocytes are associated with lymphotoxin β-producing dendritic cells in human breast cancer.* J Immunol, 2013. **191**(4): p. 2001-8.
81. Weinstein, A.M. and W.J. Storkus, *Therapeutic Lymphoid Organogenesis in the Tumor Microenvironment.* Adv Cancer Res, 2015. **128**: p. 197-233.
82. Gantsev, S.K., et al., *The role of inflammatory chemokines in lymphoid neoorganogenesis in breast cancer.* Biomed Pharmacother, 2013. **67**(5): p. 363-6.
83. Yu, P., et al., *Priming of naive T cells inside tumors leads to eradication of established tumors.* Nat Immunol, 2004. **5**(2): p. 141-9.
84. Johansson-Percival, A., et al., *De novo induction of intratumoral lymphoid structures and vessel normalization enhances immunotherapy in resistant tumors.* Nat Immunol, 2017. **18**(11): p. 1207-1217.
85. Tang, H., et al., *Facilitating T Cell Infiltration in Tumor Microenvironment Overcomes Resistance to PD-L1 Blockade.* Cancer Cell, 2016. **29**(3): p. 285-296.
86. Moyron-Quiroz, J.E., et al., *Persistence and responsiveness of immunologic memory in the absence of secondary lymphoid organs.* Immunity, 2006. **25**(4): p. 643-54.
87. Moyron-Quiroz, J.E., et al., *Role of inducible bronchus associated lymphoid tissue (iBALT) in respiratory immunity.* Nat Med, 2004. **10**(9): p. 927-34.
88. Luther, S.A., et al., *Differing activities of homeostatic chemokines CCL19, CCL21, and CXCL12 in lymphocyte and dendritic cell recruitment and lymphoid neogenesis.* J Immunol, 2002. **169**(1): p. 424-33.
89. Chen, S.C., et al., *Ectopic expression of the murine chemokines CCL21a and CCL21b induces the formation of lymph node-like structures in pancreas, but not skin, of transgenic mice.* J Immunol, 2002. **168**(3): p. 1001-8.
90. de Chaisemartin, L., et al., *Characterization of chemokines and adhesion molecules associated with T cell presence in tertiary lymphoid structures in human lung cancer.* Cancer Res, 2011. **71**(20): p. 6391-9.
91. Hamanishi, J., et al., *Activated local immunity by CC chemokine ligand 19-transduced embryonic endothelial progenitor cells suppresses metastasis of murine ovarian cancer.* Stem Cells, 2010. **28**(1): p. 164-73.
92. Schumacher, T.N. and D.S. Thommen, *Tertiary lymphoid structures in cancer.* Science, 2022. **375**(6576): p. eabf9419.

93. Sautès-Fridman, C., et al., *Tertiary Lymphoid Structures and B cells: Clinical impact and therapeutic modulation in cancer.* Semin Immunol, 2020. **48**: p. 101406.
94. Germain, C., et al., *Presence of B cells in tertiary lymphoid structures is associated with a protective immunity in patients with lung cancer.* Am J Respir Crit Care Med, 2014. **189**(7): p. 832-44.
95. Wennhold, K., et al., *CD86+ Antigen-Presenting B Cells Are Increased in Cancer, Localize in Tertiary Lymphoid Structures, and Induce Specific T-cell Responses.* Cancer Immunology Research, 2021. **9**(9): p. 1098-1108.
96. Siliņa, K., et al., *Germinal Centers Determine the Prognostic Relevance of Tertiary Lymphoid Structures and Are Impaired by Corticosteroids in Lung Squamous Cell Carcinoma.* Cancer Res, 2018. **78**(5): p. 1308-1320.
97. Allen, C.D. and J.G. Cyster, *Follicular dendritic cell networks of primary follicles and germinal centers: phenotype and function.* Semin Immunol, 2008. **20**(1): p. 14-25.
98. Fridman, W.H., et al., *B cells and tertiary lymphoid structures as determinants of tumour immune contexture and clinical outcome.* Nature Reviews Clinical Oncology, 2022. **19**(7): p. 441-457.
99. Shi, W., et al., *Follicular helper T cells promote the effector functions of CD8(+) T cells via the provision of IL-21, which is downregulated due to PD-1/PD-L1-mediated suppression in colorectal cancer.* Exp Cell Res, 2018. **372**(1): p. 35-42.
100. Niogret, J., et al., *Follicular helper-T cells restore CD8(+)-dependent antitumor immunity and anti-PD-L1/PD-1 efficacy.* J Immunother Cancer, 2021. **9**(6).
101. Goc, J., et al., *Dendritic cells in tumor-associated tertiary lymphoid structures signal a Th1 cytotoxic immune contexture and license the positive prognostic value of infiltrating CD8+ T cells.* Cancer Res, 2014. **74**(3): p. 705-15.
102. Baratin, M., et al., *T Cell Zone Resident Macrophages Silently Dispose of Apoptotic Cells in the Lymph Node.* Immunity, 2017. **47**(2): p. 349-362.e5.
103. Nayar, S., et al., *Immunofibroblasts are pivotal drivers of tertiary lymphoid structure formation and local pathology.* Proceedings of the National Academy of Sciences, 2019. **116**(27): p. 13490-13497.
104. Silva-Sanchez, A., T.D. Randall, and S. Meza-Perez, *Tertiary Lymphoid Structures Among the World of Noncanonical Ectopic Lymphoid Organizations*, in *Tertiary Lymphoid Structures: Methods and Protocols*, M.-C. Dieu-Nosjean, Editor. 2018, Springer New York: New York, NY. p. 1-15.
105. Bruno, T.C., *New predictors for immunotherapy responses sharpen our view of the tumour microenvironment.* Nature, 2020. **577**(7791): p. 474-476.
106. Carmi, Y., et al., *Allogeneic IgG combined with dendritic cell stimuli induce antitumour T-cell immunity.* Nature, 2015. **521**(7550): p. 99-104.
107. Scheel, T., et al., *V-region gene analysis of locally defined synovial B and plasma cells reveals selected B cell expansion and accumulation of plasma cell clones in rheumatoid arthritis.* Arthritis & Rheumatism, 2011. **63**(1): p. 63-72.
108. Salomonsson, S., et al., *Cellular basis of ectopic germinal center formation and autoantibody production in the target organ of patients with Sjögren's syndrome.* Arthritis & Rheumatism, 2003. **48**(11): p. 3187-3201.
109. Helmink, B.A., et al., *B cells and tertiary lymphoid structures promote immunotherapy response.* Nature, 2020. **577**(7791): p. 549-555.

110. Meylan, M., et al., *Tertiary lymphoid structures generate and propagate anti-tumor antibody-producing plasma cells in renal cell cancer.* Immunity, 2022. **55**(3): p. 527-541.e5.
111. McMahon, E.J., et al., *Epitope spreading initiates in the CNS in two mouse models of multiple sclerosis.* Nature Medicine, 2005. **11**(3): p. 335-339.
112. Wu, H., et al., *PD-L1(+) regulatory B cells act as a T cell suppressor in a PD-L1-dependent manner in melanoma patients with bone metastasis.* Mol Immunol, 2020. **119**: p. 83-91.
113. Hu, D., et al., *Artery Tertiary Lymphoid Organs Control Aorta Immunity and Protect against Atherosclerosis via Vascular Smooth Muscle Cell Lymphotoxin β Receptors.* Immunity, 2015. **42**(6): p. 1100-1115.
114. Ishigami, E., et al., *Coexistence of regulatory B cells and regulatory T cells in tumor-infiltrating lymphocyte aggregates is a prognostic factor in patients with breast cancer.* Breast Cancer, 2019. **26**(2): p. 180-189.
115. Li, R., et al., *The 12-CK Score: Global Measurement of Tertiary Lymphoid Structures.* Front Immunol, 2021. **12**: p. 694079.
116. Zhao, Z., et al., *Relationship between Tertiary Lymphoid Structure and the Prognosis and Clinicopathologic Characteristics in Solid Tumors.* Int J Med Sci, 2021. **18**(11): p. 2327-2338.
117. Bruni, D., H.K. Angell, and J. Galon, *The immune contexture and Immunoscore in cancer prognosis and therapeutic efficacy.* Nat Rev Cancer, 2020. **20**(11): p. 662-680.
118. Cabrita, R., et al., *Tertiary lymphoid structures improve immunotherapy and survival in melanoma.* Nature, 2020. **577**(7791): p. 561-565.
119. Petitprez, F., et al., *B cells are associated with survival and immunotherapy response in sarcoma.* Nature, 2020. **577**(7791): p. 556-560.
120. Cottrell, T.R., et al., *Pathologic features of response to neoadjuvant anti-PD-1 in resected non-small-cell lung carcinoma: a proposal for quantitative immune-related pathologic response criteria (irPRC).* Ann Oncol, 2018. **29**(8): p. 1853-1860.
121. Gao, J., et al., *Neoadjuvant PD-L1 plus CTLA-4 blockade in patients with cisplatin-ineligible operable high-risk urothelial carcinoma.* Nat Med, 2020. **26**(12): p. 1845-1851.
122. Vanhersecke, L., et al., *Mature tertiary lymphoid structures predict immune checkpoint inhibitor efficacy in solid tumors independently of PD-L1 expression.* Nat Cancer, 2021. **2**(8): p. 794-802.
123. Lu, Y., et al., *Complement Signals Determine Opposite Effects of B Cells in Chemotherapy-Induced Immunity.* Cell, 2020. **180**(6): p. 1081-1097.e24.
124. Ding, G.Y., et al., *Distribution and density of tertiary lymphoid structures predict clinical outcome in intrahepatic cholangiocarcinoma.* J Hepatol, 2022. **76**(3): p. 608-618.
125. Finkin, S., et al., *Ectopic lymphoid structures function as microniches for tumor progenitor cells in hepatocellular carcinoma.* Nat Immunol, 2015. **16**(12): p. 1235-44.
126. Calderaro, J., et al., *Intra-tumoral tertiary lymphoid structures are associated with a low risk of early recurrence of hepatocellular carcinoma.* J Hepatol, 2019. **70**(1): p. 58-65.
127. Posch, F., et al., *Maturation of tertiary lymphoid structures and recurrence of stage II and III colorectal cancer.* Oncoimmunology, 2018. **7**(2): p. e1378844.
128. Meylan, M., et al., *Early Hepatic Lesions Display Immature Tertiary Lymphoid Structures and Show Elevated Expression of Immune Inhibitory and Immunosuppressive Molecules.* Clin Cancer Res, 2020. **26**(16): p. 4381-4389.

129. van Dijk, N., et al., *Preoperative ipilimumab plus nivolumab in locoregionally advanced urothelial cancer: the NABUCCO trial.* Nat Med, 2020. **26**(12): p. 1839-1844.
130. Murakami, Y., et al., *Increased regulatory B cells are involved in immune evasion in patients with gastric cancer.* Sci Rep, 2019. **9**(1): p. 13083.
131. Pagliarulo, F., et al., *Molecular, Immunological, and Clinical Features Associated With Lymphoid Neogenesis in Muscle Invasive Bladder Cancer.* Front Immunol, 2021. **12**: p. 793992.
132. Berrar, D., *Performance Measures for Binary Classification*, in *Encyclopedia of Bioinformatics and Computational Biology*, S. Ranganathan, et al., Editors. 2019, Academic Press: Oxford. p. 546-560.
133. Masuda, T., et al., *Unique characteristics of tertiary lymphoid structures in kidney clear cell carcinoma: prognostic outcome and comparison with bladder cancer.* Journal for ImmunoTherapy of Cancer, 2022. **10**(3): p. e003883.
134. Koti, M., et al., *Tertiary Lymphoid Structures Associate with Tumour Stage in Urothelial Bladder Cancer.* Bladder Cancer, 2017. **3**(4): p. 259-267.
135. Hamade, A., et al., *Sex differences in the aging murine urinary bladder and influence on the tumor immune microenvironment of a carcinogen-induced model of bladder cancer.* Biol Sex Differ, 2022. **13**(1): p. 19.
136. Zemp, L., et al., *The prognostic and predictive implications of the 12-chemokine score in muscle invasive bladder cancer.* Journal of Clinical Oncology, 2021. **39**(6_suppl): p. 466-466.
137. Song, I.H., et al., *Predictive Value of Tertiary Lymphoid Structures Assessed by High Endothelial Venule Counts in the Neoadjuvant Setting of Triple-Negative Breast Cancer.* Cancer Res Treat, 2017. **49**(2): p. 399-407.
138. Deguchi, S., et al., *Clinical relevance of tertiary lymphoid structures in esophageal squamous cell carcinoma.* BMC Cancer, 2022. **22**(1): p. 699.
139. Brunet, M., et al., *Mature tertiary lymphoid structure is a specific biomarker of cancer immunotherapy and does not predict outcome to chemotherapy in non-small-cell lung cancer.* Ann Oncol, 2022. **33**(10): p. 1084-1085.
140. Sun, X., et al., *Maturation and abundance of tertiary lymphoid structures are associated with the efficacy of neoadjuvant chemoimmunotherapy in resectable non-small cell lung cancer.* Journal for ImmunoTherapy of Cancer, 2022. **10**(11): p. e005531.
141. Lin, J.R., et al., *Multiplexed 3D atlas of state transitions and immune interaction in colorectal cancer.* Cell, 2023. **186**(2): p. 363-381.e19.
142. Boackle, S.A., V.M. Holers, and D.R. Karp, *CD21 augments antigen presentation in immune individuals.* Eur J Immunol, 1997. **27**(1): p. 122-9.
143. Rocamora-Reverte, L., et al., *The Complex Role of Regulatory T Cells in Immunity and Aging.* Frontiers in Immunology, 2021. **11**.